Research Square

Preprints are preliminary reports that have not undergone peer review.
They should not be considered conclusive, used to inform clinical practice,
or referenced by the media as validated information.

Metabolic phenotypes predict survival in BCLC-C hepatocellular carcinoma receiving synchronous TACE plus targeted and immunotherapy

Liqing Li
Guangxi Medical University Cancer Hospital
Zhitao Lin
Lanzhou University
Junbao Wei
121021866@qq.com

Guangxi Medical University Cancer Hospital

Research Article

Keywords: Hepatocellular carcinoma, BCLC-C, Transarterial chemoembolization, Targeted immunotherapy, Prognostic stratification

Posted Date: September 16th, 2026

DOI: https://doi.org/10.21203/rs.3.rs-10801004/v1

License: This work is licensed under a Creative Commons Attribution 4.0 International License.
Read Full License

Additional Declarations: No competing interests reported.

Metabolic phenotypes predict survival in BCLC-C hepatocellular carcinoma receiving synchronous TACE plus targeted and immunotherapy

Liqing Li [1#], Zhitao Lin [2#], Junbao Wei [1*]

[1] Department of Radiation Oncology, Guangxi Medical University Cancer Hospital, Nanning, 530021, Guangxi, China

[2] School of Basic Medical Sciences, Lanzhou University, Lanzhou, 730000, Gansu, China

[#]Co-author

***Corresponding Author**

Liqing Li, e-mail address: liliqinglily@163.com

Zhitao Lin, e-mail address: joezhicool@outlook.com

Junbao Wei, e-mail address: 121021866@qq.com

ABSTRACT

Background: The synchronous combination of TACE, TKIs, and ICIs has improved outcomes for patients with BCLC-C HCC, yet treatment response varies widely. This study aimed to identify metabolically distinct phenotypes that predict response to synchronous triple therapy.

Methods: We conducted a retrospective cohort study of 1,792 patients with BCLC-C HCC. Propensity score matching and L2-penalized multivariate Cox regression were performed, followed by XGBoost with SHAP transformation and K-means clustering to define metabolic subtypes. Subgroup analyses with interaction testing were conducted across clinical strata to validate the robustness of the clustering system.

Results: After propensity score matching (716 pairs), synchronous triple therapy significantly improved overall survival compared with pre-immunotherapy TACE (median, 28.0 vs. 8.0 months; $P < 0.001$). Eight metabolic and clinical factors (AFP, TP, GGT, LDH, P, metastasis, HCO3, RBC) were identified as independent predictors. K-means clustering resolved four distinct metabolic phenotypes: metabolically fit (Cluster 1, 58.5%), metabolically compensated (Cluster 2, 24.6%), tumor-metabolism dominant (Cluster 3, 14.5%), and metabolically exhausted (Cluster 4, 2.4%). The metabolically fit phenotype demonstrated exceptional survival (median OS, 38.0 months; 1-year OS, 82.7%), while the metabolically exhausted phenotype showed a dismal prognosis (median OS, 4.0 months; 1-year OS, 4.2%). Subgroup analyses confirmed that the favorable prognosis of the metabolically fit phenotype remained consistent across all clinical strata.

Conclusions: The metabolic fitness-based clustering framework identifies patients with BCLC-C HCC most likely to benefit from synchronous triple therapy, suggesting that routine laboratory tests may help guide precision patient selection.

Keywords: Hepatocellular carcinoma; BCLC-C; Transarterial chemoembolization; Targeted immunotherapy; Prognostic stratification

Abbreviations

AASLD: American Association for the Study of Liver Diseases

AFP: Alpha-Fetoprotein

BCLC: Barcelona Clinic Liver Cancer

CI: Confidence Interval

CTLA-4: Cytotoxic T-Lymphocyte-Associated Antigen 4

EASL: European Association for the Study of the Liver

GGT: Gamma-Glutamyl Transferase

HCC: Hepatocellular Carcinoma

HCO3: Bicarbonate

HR: Hazard Ratio

ICI: Immune Checkpoint Inhibitor

LDH: Lactate Dehydrogenase

NLR: Neutrophil-to-Lymphocyte Ratio

OS: Overall Survival

P: Phosphorus

PCA: Principal Component Analysis

PD-1: Programmed Death-1

PD-L1: Programmed Death-Ligand 1

PSM: Propensity Score Matching

PVTT: Portal Vein Tumor Thrombus

RBC: Red Blood Cell Count

SHAP: SHapley Additive exPlanations

TACE: Transarterial Chemoembolization

TKI: Tyrosine Kinase Inhibitor

TP: Total Protein

VEGF: Vascular Endothelial Growth Factor

XGBoost: Extreme Gradient Boosting

1. INTRODUCTION

Hepatocellular carcinoma (HCC) remains the third leading cause of cancer-related mortality worldwide[1]. Among patients with HCC, those with Barcelona Clinic Liver Cancer (BCLC)-C stage disease, defined by the presence of portal vein tumor thrombus (PVTT), extrahepatic metastasis, or both, constitute a particularly challenging population with historically poor prognosis[2-4]. For decades, transarterial chemoembolization (TACE) constituted the standard locoregional therapy for patients with intermediate stage disease, yet its efficacy in BCLC-C patients was limited, with median overall survival ranging from approximately 5 to 13 months across various real-world series, depending on patient selection criteria and the proportion of patients with portal vein tumor thrombus or extrahepatic metastasis[3, 5-7].

The treatment landscape for BCLC-C hepatocellular carcinoma has undergone substantial evolution over the past decade. The initial era of molecular targeted therapy, marked by sorafenib and subsequently lenvatinib, established the feasibility of systemic disease control in advanced HCC[8, 9]. More recently, the paradigm has shifted decisively toward immune-based combination regimens, with multiple phase 3 trials demonstrating survival benefits for anti-programmed death-1 (PD-1)/programmed death-ligand 1 (PD-L1) antibodies combined with either anti-vascular endothelial growth factor (VEGF) agents or cytotoxic T-lymphocyte-associated antigen 4 (CTLA-4) inhibitors[10-12]. Beyond these established first-line standards, emerging evidence has also explored dual tyrosine kinase inhibitor (TKI) and immune checkpoint inhibitor (ICI) combinations, such as lenvatinib plus pembrolizumab and camrelizumab plus rivoceranib, further expanding the therapeutic landscape[13, 14]. In parallel, the 2026 updated guidelines from the European Association for the Study of the Liver (EASL) and the American Association for the Study of Liver Diseases (AASLD) have collectively endorsed immune-based combination therapies as the preferred first-line options for BCLC-C patients with preserved liver function, while also refining the role of TACE as a component of combination strategies for selected patients with intermediate-advanced disease[15, 16].

The biological rationale for combining TACE with systemic agents has been corroborated by multiple prospective trials. The TACTICS trial demonstrated that TACE plus sorafenib improved progression-free survival over TACE alone, while the EMERALD-1 and LEAP-012 trials have extended this paradigm to include immune checkpoint inhibitors, collectively establishing TACE plus systemic therapy as an evolving standard for selected patients with intermediate-advanced HCC[17-19].

Despite these therapeutic advances, a substantial proportion of patients with BCLC-C disease exhibit primary resistance to combination therapy, experiencing rapid disease progression despite receiving the full intended regimen[20, 21]. Current clinical staging systems and single biomarkers such as alpha-fetoprotein, while useful for prognosis and treatment allocation, do not capture the biological heterogeneity that underlies differential treatment responses among patients receiving the same therapy[2, 22-25]. This clinical reality underscores an urgent need for precision phenotyping strategies that can guide treatment selection specifically within the BCLC-C population.

Emerging evidence has highlighted the role of tumor metabolic reprogramming in shaping the tumor microenvironment and modulating responses to both targeted therapy and immunotherapy[26-28]. Circulating biomarkers that reflect these metabolic derangements and host immune-inflammatory states have been increasingly investigated as surrogate indicators of treatment response. For example, elevated lactate dehydrogenase (LDH) and pretreatment serum albumin and neutrophil-to-lymphocyte ratio (NLR), reflecting tumor glycolysis and necrosis as well as host nutritional and inflammatory states, have been associated with poor outcomes in patients receiving immune checkpoint inhibitors across multiple cancer types and specifically in hepatocellular carcinoma[29-31]. However, whether a comprehensive metabolic phenotyping approach using widely available blood tests can effectively stratify patients with BCLC-C HCC according to their likelihood of benefiting from synchronous TACE plus targeted immunotherapy remains to be established.

In this study, we therefore aimed to develop a metabolic phenotyping framework using routine blood tests and clinical assessment to stratify patients with BCLC-C HCC receiving

synchronous triple therapy (TACE, TKIs, and ICIs), with the goal of enabling precision patient selection in clinical practice.

2. METHODS

2.1. Study Design and Patient Population

This retrospective cohort study was conducted using electronic medical records from patients diagnosed with hepatocellular carcinoma at our institution between December 2015 and December 2025. The study protocol was approved by the institutional review board, and the requirement for informed consent was waived given the retrospective nature of the analysis.

By the time of the study period, targeted therapies had already been incorporated into clinical practice for patients with advanced HCC at our institution, whereas the combination of tyrosine kinase inhibitors (TKIs) and immune checkpoint inhibitors (ICIs) had not yet been routinely adopted before 2019. After 2019, with the advent of the targeted immunotherapy era, we began to administer synchronous TACE combined with TKIs and PD-1/PD-L1 inhibitors in eligible patients. For the purposes of this retrospective analysis, we restricted the combination therapy cohort to patients in whom TKIs and ICIs were initiated within seven days after the first TACE session and prior to hospital discharge, with no treatment gap between locoregional and systemic therapies, to ensure therapeutic homogeneity.

Eligible patients had a confirmed diagnosis of BCLC-C stage HCC and received either TACE (with or without TKIs, but without ICIs) between 2015 and 2018, or synchronous TACE combined with TKIs and ICIs between 2019 and 2025 meeting the above time-window criteria. Patients receiving TACE-based therapy without ICIs after 2019 were excluded from the comparator group to avoid selection bias, as such patients typically had undocumented contraindications to immunotherapy, including poor performance status, severe hepatic decompensation, post-TACE complications, or financial constraints. Patients who initiated TKIs or ICIs more than seven days after TACE or after discharge were also excluded.

Additional exclusion criteria included missing survival timelines, loss to follow-up, and conflicting stage classifications. Patients were further categorized by disease status as primary HCC (no prior history of hepatectomy, ablation, or TACE) or recurrent HCC (prior curative-intent therapies or prior TACE sessions with subsequent intrahepatic recurrence).

2.2 Propensity Score Matching

To minimize confounding by indication between the two treatment eras, 1:1 nearest-neighbor propensity score matching (PSM) was performed using a caliper of 0.02. The propensity score was calculated from a logistic regression model that incorporated the following baseline covariates: age, sex, PVTT status, distant metastasis status, recurrence status, alpha-fetoprotein (AFP), albumin, total bilirubin, creatinine, red blood cell count (RBC), total protein, and neutrophil-to-lymphocyte ratio (NLR).

Metabolic and electrolyte parameters, including anion gap, bicarbonate, lactate dehydrogenase (LDH), gamma-glutamyl transferase (GGT), calcium, phosphorus, magnesium, potassium, and chloride, were intentionally excluded from the propensity score model. These variables were considered on-treatment mediators rather than baseline confounders, as TKIs directly modulate renal electrolyte handling and tumor glycolytic metabolism. Adjusting for these mediators would constitute overadjustment, which may bias the estimated treatment effect toward the null.

2.3 Data Preprocessing, Imputation, and Feature Selection

Variables with a missing rate exceeding 20% were excluded from the analysis. Missing continuous variables were imputed using the K-nearest neighbors algorithm with K equal to 5. Univariate Cox proportional hazards analysis was initially applied to screen all clinical and biochemical parameters. Variables achieving a P value below 0.05 were subsequently entered into a multivariate Cox model incorporating an L2 regularization penalty, with a penalizer parameter of 0.05, to mitigate the effects of multicollinearity inherent in complex metabolic indices.

To enable direct comparison of effect sizes across biomarkers measured on different scales, all continuous variables were standardized to z-scores (mean = 0, standard deviation = 1) prior to entry into the multivariate Cox model. This transformation ensures that the resulting hazard ratios represent the change in mortality risk associated with a 1-standard deviation (SD) increase in each predictor, allowing meaningful comparison of prognostic impact across variables with disparate units (e.g., ng/mL for AFP vs. U/L for LDH). The standardization was performed on the imputed dataset, and the same scaling parameters were applied consistently across all analyses.

Features retained as independent predictors in the final multivariate model, defined by a P value below 0.05, were designated as the core feature set for subsequent machine learning analyses. For clustering, however, variables were used on their original continuous scale (rather than standardized z-scores) to preserve the full dynamic range of extreme values, which is critical for separating metabolically distinct phenotypes.

2.4 SHAP-Driven XGBoost and K-Means Clustering

An Extreme Gradient Boosting (XGBoost) survival regressor with the objective function set to survival:cox was trained on the core feature set. To achieve individual-level interpretability and to overcome the black box limitation of machine learning, the model output was deconstructed using the TreeExplainer algorithm to generate a SHapley Additive exPlanations (SHAP) value matrix for each patient, quantifying the directional impact of each feature on mortality risk at the individual level. This SHAP matrix was used as the topological input for K-means unsupervised clustering to identify natural patient subgroups. The optimal number of clusters was evaluated across a range from 2 to 10, balancing the Elbow method based on inertia minimization, the Silhouette score, and clinical interpretability, defined by the distinct separation of Kaplan-Meier survival curves with a significant log-rank P value.

2.5 Subgroup Interaction Analysis

To evaluate whether the prognostic stratification power of the identified clusters was consistent across heterogeneous clinical scenarios, subgroup interaction analyses were

performed. Patients were stratified according to six baseline clinical domains: recurrence status (primary vs. recurrent HCC), PVTT status (absent vs. present), distant metastasis (absent vs. present), baseline AFP level (<400 vs. ≥400 ng/mL), age group (<60 vs. ≥60 years), and gender (female vs. male). Within each stratum, hazard ratios and 95% confidence intervals were calculated using multivariate Cox proportional hazards regression, adjusting for all covariates included in the core feature set. To formally test for effect modification, multiplicative interaction terms (cluster phenotype × subgroup covariate) were introduced into the Cox regression models. A P value for interaction greater than 0.05 was considered to indicate no significant effect modification. Results were visualized using forest plots, with separate figures constructed for the favorable phenotype (Cluster 1 vs. others) and the extreme high-risk phenotype (Cluster 4 vs. others).

2.6 Statistical Analysis

Continuous variables were compared using the Student t test or the Mann-Whitney U test, as appropriate. Categorical variables were compared using the chi-square test. Survival curves were estimated using the Kaplan-Meier method and compared using the log-rank test. All statistical analyses were conducted using Python, with the Scikit-learn, Lifelines, and SHAP libraries. A two-sided P value below 0.05 was considered statistically significant.

3. RESULTS

3.1 Overall Survival Benefit of Synchronous Triple Therapy in BCLC-C Patients

Before propensity score matching, substantial baseline imbalances were observed between the pre-immunotherapy TACE group and the synchronous triple-therapy group. Patients in the triple-therapy group had a higher proportion of recurrent disease (27.9% vs. 5.8%, P < 0.001) and higher median AFP levels (3,653.5 vs. 815.1 ng/mL, P < 0.001), while the pre-immunotherapy TACE group had a higher proportion of patients with distant metastasis (24.0% vs. 17.8%, P = 0.001). Complete baseline characteristics before and after matching are

presented in **Table S1**. The Kaplan-Meier analysis before matching demonstrated significantly superior survival for the triple-therapy group (log-rank P < 0.001; **Figure 1A**).

After 1:1 propensity score matching using the 12 predefined covariates, 716 well-balanced pairs were generated. All matched covariates were effectively balanced, with P values exceeding 0.05 for all variables. Importantly, metabolic and electrolyte parameters, including anion gap, bicarbonate, calcium, phosphorus, potassium, and LDH, remained significantly different between the two groups after matching, with P values below 0.05 for all comparisons. This observation confirmed our methodological decision to exclude these variables from the propensity score model, as their persistent imbalance reflects their status as treatment-induced mediators rather than baseline confounders.

Kaplan-Meier analysis of the matched cohort demonstrated that patients receiving synchronous triple therapy experienced significantly superior overall survival compared with those in the pre-immunotherapy TACE group (log-rank P < 0.001; **Figure 1B; Table S2**). In the synchronous triple-therapy group, the median overall survival was 28.0 months (95% CI, 26.0-35.0 months), compared with 8.0 months (95% CI, 7.0-9.0 months) in the TACE-only group. The 5-year overall survival rate was 36.7% (95% CI, 31.7-41.6%) in the combination group and 8.0% (95% CI, 6.1-10.1%) in the TACE-only group.

3.2 Identification of Eight Independent Prognostic Biomarkers

To isolate the core prognostic drivers from the large number of collinear clinical and biochemical variables, we applied L2-penalized multivariate Cox regression. The results of the univariate and multivariate analyses are presented in **Table 1**. After regularization, eight features were retained as independent predictors of overall survival.

AFP demonstrated a hazard ratio (HR) of 1.178 (95% confidence interval [CI]: 1.097–1.266; P < 0.001). Total protein (TP) was identified as a protective factor (HR, 0.846; 95% CI: 0.760–0.940; P = 0.002). GGT was associated with increased mortality risk (HR, 1.130; 95% CI: 1.026–1.245; P = 0.013). LDH also demonstrated an increased risk (HR, 1.140; 95% CI: 1.024–1.271; P = 0.017). Phosphorus (P) emerged as a protective factor (HR, 0.882; 95% CI: 0.794–

0.980; P = 0.019). The presence of distant metastasis was associated with increased risk (HR, 1.329; 95% CI: 1.035–1.705; P = 0.026). Bicarbonate (HCO3) demonstrated that lower levels were associated with worse survival (HR, 1.170; 95% CI: 1.012–1.353; P = 0.034). Finally, RBC was identified as a protective factor (HR, 0.874; 95% CI: 0.765–0.999; P = 0.048).

The retention of LDH, HCO3, and P alongside AFP, GGT, TP, and RBC underscores the critical role of tumor glycolytic activity, acid-base homeostasis, nutritional reserve, and anemia in determining resistance to TACE plus targeted immunotherapy. Notably, distant metastasis exhibited the largest risk amplification (HR, 1.329), followed by AFP (HR, 1.178) and HCO3 (HR, 1.170), while TP (HR, 0.846) and RBC (HR, 0.874) conferred the most substantial protective effects.

3.3 Determination of the Optimal Clustering Configuration

To stratify the heterogeneous cohort, we transformed the eight core features into a SHAP value matrix and subjected this matrix to K-means unsupervised clustering. The evaluation of cluster compactness, assessed by inertia, and cluster separation, assessed by the Silhouette score, was performed across values of K ranging from 2 to 10, as shown in **Figure 2**. The inertia curve demonstrated a distinct elbow at K equal to 4, and the Silhouette score confirmed optimal separation at this configuration. The four-cluster solution produced four sharply demarcated, non-overlapping Kaplan-Meier curves representing a continuous prognostic spectrum ranging from favorable to extreme high-risk, with a log-rank P value below 0.001. Accordingly, K equal to 4 was definitively selected as the optimal clustering configuration.

3.4 PCA and Survival Disparities Validate Subtype Integrity

Principal component analysis (PCA) of the SHAP space demonstrated robust spatial segregation of the four clusters, with distinct confidence ellipses confirming the structural integrity of the classification (**Figure 3A**). The Kaplan-Meier survival analysis revealed a stepwise survival gradient across the four clusters (**Figure 3B; Table 2**). Cluster 1 comprised 586 patients (58.5%) and demonstrated the best prognosis, with a median overall survival (OS) of 38.0 months (95% CI, 31.0-55.0) and a 5-year OS rate of 42.7% (95% CI, 36.8-48.6). Cluster

2, comprising 246 patients (24.6%), showed an intermediate-favorable prognosis (median OS, 21.0 months; 5-year OS, 28.6%). Cluster 3, comprising 145 patients (14.5%), demonstrated an intermediate-poor prognosis (median OS, 15.0 months; 5-year OS, 23.1%). Cluster 4, comprising only 24 patients (2.4%), exhibited a dismal prognosis (median OS, 4.0 months; 1-year OS, 4.2%).

3.5 Phenotypic Architecture of the Four Clusters

Radar plots (**Figure 4A**) and cluster-specific SHAP signature centers (**Figure 4B**) revealed distinct metabolic profiles across the four clusters. Cluster 1 was characterized by a coordinated pattern of preserved hepatic and metabolic function, with low tumor burden markers and normal acid-base balance. Cluster 2 showed a profile of mild metabolic derangement, primarily driven by modest elevations in GGT and LDH. Cluster 3 exhibited a discordant profile with high AFP and LDH but preserved total protein and bicarbonate, suggesting a state of high tumor metabolic demand without complete host decompensation. Cluster 4 displayed a convergent profile of maximal tumor burden markers, suppressed bicarbonate, and depleted nutritional reserves, consistent with a state of global metabolic failure.

3.6 SHAP Global and Event-Stratified Interpretability

The SHAP global summary plot (**Figure 5A**) ranked features by their impact on mortality risk. High AFP, GGT, LDH, and distant metastasis shifted patients into positive SHAP territory (increased risk), while high total protein, phosphorus, RBC, and bicarbonate conferred protection (negative SHAP values). When stratified by clinical endpoint, deceased patients were concentrated in high-positive SHAP domains, driven by extreme AFP and LDH elevations and suppressed bicarbonate, total protein, phosphorus, and RBC.

Cluster-specific SHAP trajectory facets (**Figure 5B**) confirmed that the metabolically fit phenotype was consistently associated with protective (negative) SHAP contributions across all features, whereas the metabolically exhausted phenotype demonstrated risk-increasing (positive) SHAP contributions for AFP, GGT, LDH, and metastasis.

3.7 Subgroup Validation Confirms Robustness Across Clinical Strata

Subgroup analyses using forest plots (**Figure 6, Figure S1-3; Tables S3-S6**) validated the robustness of the four-cluster classification across diverse clinical subgroups. Compared with other clusters, the metabolically fit phenotype was associated with a significantly reduced mortality risk (HR, 0.44; 95% CI, 0.37-0.53; P < 0.001), and this protective effect remained consistent across subgroups defined by recurrence status (P for interaction = 0.182), PVTT (P = 0.277), distant metastasis (P = 0.463), AFP level (P = 0.616), age (P = 0.597), and gender (P = 0.101) (**Figures 6**). In contrast, the metabolically exhausted phenotype conferred a markedly increased mortality risk (HR range, 4.57-10.13), with consistent effect sizes across most subgroups (all P for interaction > 0.05), except for a potential sex-specific interaction (P = 0.025) (**Figures S3**). Clusters 2 and 3 demonstrated intermediate risk profiles, with HRs of 1.47 (95% CI, 1.19-1.81) and 1.80 (95% CI, 1.45-2.25), respectively, relative to other clusters (**Figures S1, S2**). These findings indicate that the SHAP-derived four-cluster classification captures intrinsic biological fitness beyond conventional clinical covariates, with particularly robust performance for the metabolically fit phenotype.

4. DISCUSSION

In the propensity-matched cohort, patients receiving synchronous triple therapy achieved a median overall survival of 28.0 months, compared with 8.0 months in the pre-immunotherapy TACE group, confirming a substantial survival benefit of this combination regimen in BCLC-C disease. However, this average treatment effect masks considerable interpatient heterogeneity. The four metabolic phenotypes identified by our clustering framework, ranging from metabolically fit to metabolically exhausted, demonstrate that patients receiving the same intensive regimen can have profoundly different outcomes. These findings carry potential clinical implications. The eight features comprising the clustering framework are all routine, low-cost, and universally available tests that could be readily integrated into baseline assessments. Patients with the metabolically fit phenotype may be the most suitable candidates for standard triple therapy, whereas those with the metabolically exhausted phenotype, who

appeared to derive minimal benefit, may be candidates for alternative strategies, including clinical trials of novel agents or best supportive care.

It is worth noting that the observed median survival of 28.0 months in the triple-therapy group warrants careful interpretation. This magnitude of benefit is consistent with, though at the higher end of, findings from recent clinical trials and large real-world studies[17-19, 32, 33]. We acknowledge that this estimate appears favorable relative to historical BCLC-C benchmarks[2, 5, 22, 34], and several factors likely contribute to this observation. First, our cohort exclusively comprised patients who tolerated immediate post-TACE initiation of TKIs and ICIs, inherently excluding those with early treatment-related complications or severely compromised hepatic reserve. Second, the contemporary era benefited from improved supportive care, including antiviral therapy, nutritional support, and optimized adverse event management, which may have contributed to survival prolongation beyond the direct antitumor effects of the combination regimen. Third, the inclusion of patients with recurrent HCC (27.9% of the triple-therapy cohort) may introduce a degree of healthy survivor bias, as these patients had already demonstrated favorable disease biology by surviving prior treatments. Consequently, our survival estimates should be interpreted as reflecting outcomes in a carefully selected, treatment-tolerant subset of BCLC-C patients rather than the entire BCLC-C population. External validation in more broadly inclusive cohorts is warranted.

The identification of four distinct prognostic subtypes within the triple-therapy cohort reveals that the average treatment effect masks substantial interpatient variability. This observation underscores the limitations of the current one-size-fits-all approach and highlights the urgent need for precision stratification strategies specifically designed for the BCLC-C population. Although conventional tumor burden indicators (AFP and metastasis) were included in the feature matrix, our clustering system is conceptually framed as a metabolic phenotyping strategy. This is because AFP and metastasis represent the tumor-side drivers of metabolic stress, while LDH, bicarbonate, phosphorus, total protein, and RBC collectively reflect the host-side buffering capacity against glycolysis-derived acidosis, nutritional exhaustion, and

anemia. Thus, the four identified clusters depict a graded spectrum of systemic host-metabolic fitness in response to tumor burden.

The most clinically significant finding of our study is the identification of the metabolically fit phenotype (Cluster 1), which comprised 58.5% of patients and achieved a median overall survival of 38.0 months and a 5-year survival rate of 42.7%. These survival outcomes are exceptional for patients with BCLC-C disease and approach those observed in patients with earlier stage disease receiving curative-intent therapy. This phenotype was characterized by low AFP, GGT, and LDH; preserved total protein; normal bicarbonate; adequate phosphorus; normal RBC; and low metastasis burden. Importantly, the favorable prognosis associated with Cluster 1 was consistently observed across all clinical subgroups, including patients with PVTT, distant metastasis, recurrent disease, and high AFP. This consistency across diverse clinical contexts confirms that our metabolic subtyping captures intrinsic biological fitness beyond conventional clinical covariates.

Conversely, the metabolically exhausted phenotype (Cluster 4), comprising only 2.4% of patients, represents a unique metabolic catastrophe phenotype characterized by extreme tumor burden, massive glycolysis and necrosis, severe acidosis, nutritional exhaustion, and anemia. Patients in this cluster derived virtually no survival benefit from synchronous triple therapy, with a median overall survival of only 4.0 months and a 1-year survival rate of 4.2%. These outcomes are worse than those observed in historical TACE-only cohorts, suggesting that this phenotype represents a state of absolute refractoriness to current standard-of-care combination therapy. The extreme mortality risk associated with Cluster 4 was consistently observed across all clinical subgroups, with hazard ratios ranging from 4.57 to 10.13 relative to other clusters. This finding has direct clinical implications: patients with this phenotype should be considered for alternative therapeutic strategies, including dual immunotherapy combinations, enrollment in clinical trials of novel agents, or best supportive care to avoid futile aggressive therapy.

Among the independent prognostic factors, LDH, HCO3, and P form a metabolic axis closely linked to the Warburg effect and systemic acid-base balance[35-37]. Elevated LDH reflects extensive tumor glycolysis and lactate accumulation, which has been shown to impair CD8-

positive T lymphocyte function and reduce the cellular uptake of weakly basic TKIs through pH-dependent ion trapping[38-40]. Low HCO3, in turn, may indicate exhausted systemic buffering capacity against tumor-derived acid load[41, 42]. The concurrent elevation of LDH and suppression of HCO3, as observed in the metabolically exhausted phenotype, suggests a state of tumor-driven metabolic acidosis that may contribute to immune evasion and therapeutic resistance[39, 43-45]. In contrast, higher P levels were associated with improved survival in our multivariate model. P depletion in advanced cancer patients often reflects poor nutritional status and depleted ATP reserves; its preservation may therefore serve as a marker of metabolic resilience rather than a direct mediator of treatment response[46-48].

Beyond the LDH-HCO3-P axis, TP and RBC were identified as additional protective factors. TP, which encompasses both albumin and globulins, may reflect not only nutritional status but also humoral immune competence[49, 50]. RBC count, while traditionally viewed as a marker of anemia, may influence outcomes through tissue oxygen delivery and physical performance reserve[51, 52]. Notably, the metabolically fit phenotype (Cluster 1) demonstrated a coordinated pattern of preserved metabolic function across multiple dimensions, suggesting that patients with this phenotype possess sufficient host metabolic reserve to tolerate and respond to intensive triple therapy.

Several limitations of this study should be acknowledged. First, this was a retrospective, single-center study, which introduces inherent selection bias, as the cohort was derived from a single institution. Second, the small sample size of Cluster 4 (n=24) limits the precision of our estimates for this extreme high-risk group, although the consistency of findings across diverse clinical subgroups supports the robustness of this phenotype. Third, the clustering model was developed and evaluated using the full cohort without a separate external validation set, which may limit the generalizability of our findings. Fourth, there may be unmeasured confounders, including performance status, Child-Pugh score details, and etiology of liver disease. Future external validation in multicenter cohorts and prospective trials is warranted to confirm the applicability of the four-cluster model.

5. CONCLUSION

The SHAP-driven clustering framework stratifies patients with BCLC-C HCC receiving synchronous TACE plus targeted immunotherapy into four prognostically distinct metabolic phenotypes, suggesting that routine blood tests may aid in identifying patients most likely to benefit from intensive triple therapy.

DECLARATIONS

Ethics approval and consent to participate： This retrospective cohort study was conducted in accordance with the Declaration of Helsinki and was approved by the Institutional Review Board of Guangxi Medical University Cancer Hospital (approval number: KY2026815), which also approved the waiver of informed consent due to the retrospective nature of the study.

Consent for publication： Not applicable.

Availability of data and materials： The datasets used during the current study are available from the corresponding author on reasonable request.

Competing interests： The authors declare that they have no competing interests.

Funding： This research received no specific grant from any funding agency in the public, commercial, or not for profit sectors.

Authors' contributions: Conceptualization: L. Li and W. Wei; Data curation: L. Li and Z. Lin; Formal analysis: L. Li; Methodology: L. Li and W. Wei; Project administration: W. Wei and Z. Lin; Resources: S. Liang and W. Wei; Software: L. Li; Visualization: L. Li; Writing-original draft: L. Li and S. Liang; Writing-review & editing: all authors. All authors read and approved the final manuscript.

Acknowledgements： Not applicable.

References

1. Filho AM, Laversanne M, Ferlay J, Colombet M, Pineros M, Znaor A, Parkin DM, Soerjomataram I, Bray F: **The GLOBOCAN 2022 cancer estimates: Data sources, methods, and a snapshot of the cancer burden worldwide**. *Int J Cancer* 2025, **156**(7):1336-1346.
2. Vogel A, Meyer T, Sapisochin G, Salem R, Saborowski A: **Hepatocellular carcinoma**. *Lancet* 2022, **400**(10360):1345-1362.
3. Usman Younas M, Saeed A, Ramzan M, Junaid Tahir M, Abbasher Hussien Mohamed Ahmed K, Ahmed A: **Transarterial chemoembolization in hepatocellular carcinoma: exploring its role in vascular invasion and extrahepatic metastasis: A systematic review**. *Medicine (Baltimore)* 2025, **104**(8):e41570.
4. Minagawa M, Makuuchi M: **Treatment of hepatocellular carcinoma accompanied by portal vein tumor thrombus**. *World J Gastroenterol* 2006, **12**(47):7561-7567.
5. Park JW, Kim YJ, Kim DY, Bae SH, Paik SW, Lee YJ, Kim HY, Lee HC, Han SY, Cheong JY *et al*: **Sorafenib with or without concurrent transarterial chemoembolization in patients with advanced hepatocellular carcinoma: The phase III STAH trial**. *J Hepatol* 2019, **70**(4):684-691.
6. Llovet JM, Real MI, Montana X, Planas R, Coll S, Aponte J, Ayuso C, Sala M, Muchart J, Sola R *et al*: **Arterial embolisation or chemoembolisation versus symptomatic treatment in patients with unresectable hepatocellular carcinoma: a randomised controlled trial**. *Lancet* 2002, **359**(9319):1734-1739.
7. Zhang X, Wang K, Wang M, Yang G, Ye X, Wu M, Cheng S: **Transarterial chemoembolization (TACE) combined with sorafenib versus TACE for hepatocellular carcinoma with portal vein tumor thrombus: a systematic review and meta-analysis**. *Oncotarget* 2017, **8**(17):29416-29427.
8. Kudo M, Finn RS, Qin S, Han KH, Ikeda K, Piscaglia F, Baron A, Park JW, Han G, Jassem J *et al*: **Lenvatinib versus sorafenib in first-line treatment of patients with unresectable hepatocellular carcinoma: a randomised phase 3 non-inferiority trial**. *Lancet* 2018, **391**(10126):1163-1173.
9. Llovet JM, Ricci S, Mazzaferro V, Hilgard P, Gane E, Blanc JF, de Oliveira AC, Santoro A, Raoul JL, Forner A *et al*: **Sorafenib in advanced hepatocellular carcinoma**. *N Engl J Med* 2008, **359**(4):378-390.
10. Ren Z, Xu J, Bai Y, Xu A, Cang S, Du C, Li Q, Lu Y, Chen Y, Guo Y *et al*: **Sintilimab plus a bevacizumab biosimilar (IBI305) versus sorafenib in unresectable hepatocellular carcinoma (ORIENT-32): a randomised, open-label, phase 2-3 study**. *Lancet Oncol* 2021, **22**(7):977-990.
11. Finn RS, Qin S, Ikeda M, Galle PR, Ducreux M, Kim TY, Kudo M, Breder V, Merle P, Kaseb AO *et al*: **Atezolizumab plus Bevacizumab in Unresectable Hepatocellular Carcinoma**. *N Engl J Med* 2020, **382**(20):1894-1905.
12. Sangro B, Galle PR, Kelley RK, Charoentum C, De Toni EN, Ostapenko Y, Heo J, Cheng AL, Wilson Woods A, Gupta C *et al*: **Patient-Reported Outcomes From the Phase III HIMALAYA Study of Tremelimumab Plus Durvalumab in Unresectable Hepatocellular Carcinoma**. *J Clin Oncol* 2024, **42**(23):2790-2799.

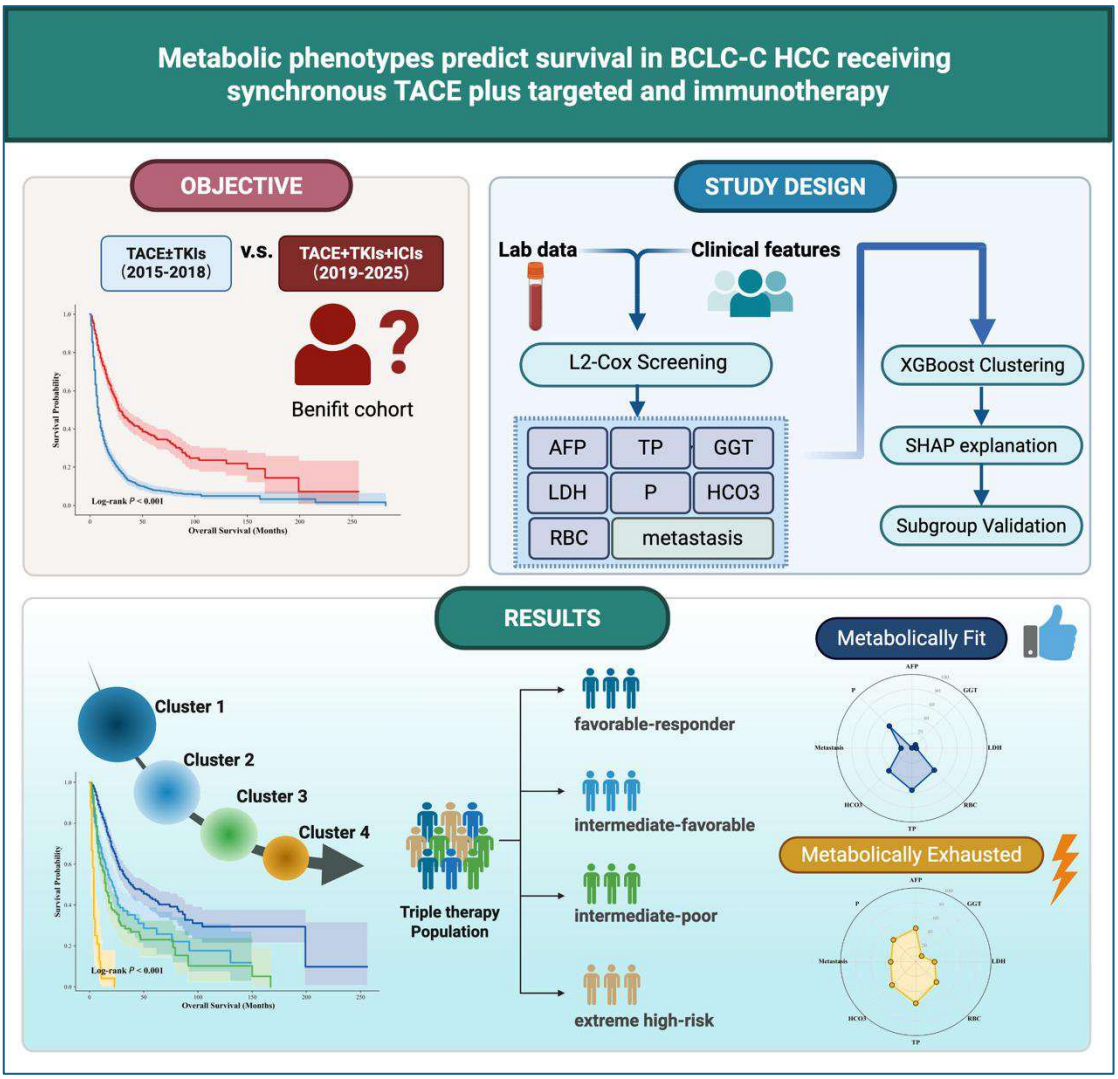
13. Finn RS, Ikeda M, Zhu AX, Sung MW, Baron AD, Kudo M, Okusaka T, Kobayashi M, Kumada H, Kaneko S *et al*: **Phase Ib Study of Lenvatinib Plus Pembrolizumab in Patients With Unresectable Hepatocellular Carcinoma**. *J Clin Oncol* 2020, **38**(26):2960-2970.
14. Qin S, Chan SL, Gu S, Bai Y, Ren Z, Lin X, Chen Z, Jia W, Jin Y, Guo Y *et al*: **Camrelizumab plus rivoceranib versus sorafenib as first-line therapy for unresectable hepatocellular carcinoma (CARES-310): a randomised, open-label, international phase 3 study**. *Lancet* 2023, **402**(10408):1133-1146.
15. European Association for the Study of the L: **EASL Clinical Practice Guidelines on the management of hepatocellular carcinoma**. *J Hepatol* 2025, **82**(2):315-374.
16. Taddei TH, Brown DB, Yarchoan M, Mendiratta-Lala M, Llovet JM: **Critical Update: AASLD Practice Guidance on prevention, diagnosis, and treatment of hepatocellular carcinoma**. *Hepatology* 2025, **82**(1):272-274.
17. Kudo M, Ueshima K, Ikeda M, Torimura T, Tanabe N, Aikata H, Izumi N, Yamasaki T, Nojiri S, Hino K *et al*: **Randomised, multicentre prospective trial of transarterial chemoembolisation (TACE) plus sorafenib as compared with TACE alone in patients with hepatocellular carcinoma: TACTICS trial**. *Gut* 2020, **69**(8):1492-1501.
18. Sangro B, Kudo M, Erinjeri JP, Qin S, Ren Z, Chan SL, Arai Y, Heo J, Mai A, Escobar J *et al*: **Durvalumab with or without bevacizumab with transarterial chemoembolisation in hepatocellular carcinoma (EMERALD-1): a multiregional, randomised, double-blind, placebo-controlled, phase 3 study**. *Lancet* 2025, **405**(10474):216-232.
19. Kudo M, Ren Z, Guo Y, Han G, Lin H, Zheng J, Ogasawara S, Kim JH, Zhao H, Li C *et al*: **Transarterial chemoembolisation combined with lenvatinib plus pembrolizumab versus dual placebo for unresectable, non-metastatic hepatocellular carcinoma (LEAP-012): a multicentre, randomised, double-blind, phase 3 study**. *Lancet* 2025, **405**(10474):203-215.
20. Lombardi P, Ramon-Gil E, Raja RQ, Brunetti L, Manfredi GF, Zhou Z, Merces G, Cappuyns S, Maria Fulgenzi CA, D'Alessio A *et al*: **A myeloid immunosuppressive phenotype defines primary refractoriness to atezolizumab plus bevacizumab in hepatocellular carcinoma**. *J Hepatol* 2026.
21. Kaseb AO, Guan Y, Gok Yavuz B, Abbas AR, Lu S, Hasanov E, Toh HC, Verret W, Wang Y: **Serum IGF-1 Scores and Clinical Outcomes in the Phase III IMbrave150 Study of Atezolizumab Plus Bevacizumab versus Sorafenib in Patients with Unresectable Hepatocellular Carcinoma**. *J Hepatocell Carcinoma* 2022, **9**:1065-1079.
22. Reig M, Forner A, Rimola J, Ferrer-Fabrega J, Burrel M, Garcia-Criado A, Kelley RK, Galle PR, Mazzaferro V, Salem R *et al*: **BCLC strategy for prognosis prediction and treatment recommendation: The 2022 update**. *J Hepatol* 2022, **76**(3):681-693.
23. Galle PR, Foerster F, Kudo M, Chan SL, Llovet JM, Qin S, Schelman WR, Chintharlapalli S, Abada PB, Sherman M *et al*: **Biology and significance of alpha-fetoprotein in hepatocellular carcinoma**. *Liver Int* 2019, **39**(12):2214-2229.

24. Llovet JM, Montal R, Sia D, Finn RS: **Molecular therapies and precision medicine for hepatocellular carcinoma**. *Nat Rev Clin Oncol* 2018, **15**(10):599-616.
25. Schulze K, Imbeaud S, Letouze E, Alexandrov LB, Calderaro J, Rebouissou S, Couchy G, Meiller C, Shinde J, Soysouvanh F *et al*: **Exome sequencing of hepatocellular carcinomas identifies new mutational signatures and potential therapeutic targets**. *Nat Genet* 2015, **47**(5):505-511.
26. Wu G, Fan X, Cheng L, Chen Z, Yi Y, Liang J, Huang X, Yang N, Yin J, Guo W *et al*: **Metabolism-driven posttranslational modifications and immune regulation: Emerging targets for immunotherapy**. *Sci Adv* 2025, **11**(37):eadx6489.
27. Lv Y, Li Z, Liu S, Zhou Z, Song J, Ba Y, Weng S, Zuo A, Xu H, Luo P *et al*: **Metabolic checkpoints in immune cell reprogramming: rewiring immunometabolism for cancer therapy**. *Mol Cancer* 2025, **24**(1):210.
28. Zhang H, Fan J, Kong D, Sun Y, Zhang Q, Xiang R, Lu S, Yang W, Feng L, Zhang H: **Immunometabolism: crosstalk with tumor metabolism and implications for cancer immunotherapy**. *Mol Cancer* 2025, **24**(1):249.
29. Midik MM, Gunenc D, Acar PF, Karaca BS: **Prognostic Value of Blood-Based Inflammatory Markers in Cancer Patients Receiving Immune Checkpoint Inhibitors**. *Cancers (Basel)* 2024, **17**(1).
30. Felismino T, Martins L, Barroso M, Carvalho D, Brito A, Maccali C, Coimbra F: **Neutrophil-to-Lymphocyte Ratio (NLR) as a Predictive Biomarker in Advanced Hepatocellular Carcinoma Treated with First-Line Immunotherapy**. *J Gastrointest Cancer* 2025, **56**(1):175.
31. Fu J, Peng W, Jiang J, Deng T, Duan H, Liu K: **Prognostic nutritional index and the survival of patients with hepatocellular carcinoma on immune checkpoint inhibitors: a meta-analysis**. *BMC Cancer* 2025, **26**(1):62.
32. Zhao Y, Wen S, Xue Y, Dang Z, Nan Z, Wang D, Li X, Feng D, Chen Y: **Transarterial chemoembolization combined with lenvatinib plus tislelizumab for unresectable hepatocellular carcinoma: a multicenter cohort study**. *Front Immunol* 2024, **15**:1449663.
33. Han F, Wang XH, Xu CZ: **Clinical benefits of transarterial chemoembolization combined with tyrosine kinase and immune checkpoint inhibitors for unresectable hepatocellular carcinoma**. *World J Gastrointest Oncol* 2024, **16**(7):3308-3320.
34. Lin CW, Chen YS, Lo GH, Wu TC, Yeh JH, Yeh ML, Dai CY, Huang JF, Chuang WL, Roberts L *et al*: **Resubclassification and clinical management for Barcelona Clinic Liver Cancer Stage C hepatocellular carcinoma**. *Hepatol Int* 2021, **15**(4):946-956.
35. Wang X, Xiong D, Cui S, Duan B, Ding G, Huang Y, Wang Q: **Lactate signaling and immune suppression in tumors: mechanisms and therapeutic implications**. *Cell Oncol (Dordr)* 2026, **49**(3).
36. Chen J, Huang Z, Chen Y, Tian H, Chai P, Shen Y, Yao Y, Xu S, Ge S, Jia R: **Lactate and lactylation in cancer**. *Signal Transduct Target Ther* 2025, **10**(1):38.
37. Xu Y, Hao X, Ren Y, Xu Q, Liu X, Song S, Wang Y: **Research progress of abnormal lactate metabolism and lactate modification in immunotherapy of hepatocellular carcinoma**. *Front Oncol* 2022, **12**:1063423.

38. Li J, Yang W, Xin T, Zhou Z, Liu X, Tang P, An J, Ma B, Peng F: **Roles of lactate and lactylation in tumor immune suppression and drug resistance**. *Front Immunol* 2026, **17**:1836534.
39. Di Carlo E: **Targeting the cancer metabolism-immunity interface: update and perspectives**. *Exp Hematol Oncol* 2026.
40. Hrabeta J, Belhajova M, Subrtova H, Merlos Rodrigo MA, Heger Z, Eckschlager T: **Drug Sequestration in Lysosomes as One of the Mechanisms of Chemoresistance of Cancer Cells and the Possibilities of Its Inhibition**. *Int J Mol Sci* 2020, **21**(12).
41. Chai D, Yang T, Zhang L, Hui Y, Feng J, Wang W: **Prognostic value of the lactate dehydrogenase to albumin ratio in cancer patients**. *Front Nutr* 2025, **12**:1610487.
42. Li X, Tang L, Cao J, Liu Y: **The inhibitory effect of hepatic cancer energy metabolism on immune checkpoint therapy: perspectives from single-cell multi-omics analysis**. *Front Immunol* 2026, **17**:1753670.
43. Peng X, He Z, Yuan D, Liu Z, Rong P: **Lactic acid: The culprit behind the immunosuppressive microenvironment in hepatocellular carcinoma**. *Biochim Biophys Acta Rev Cancer* 2024, **1879**(5):189164.
44. Bogdanov A, Bogdanov A, Chubenko V, Volkov N, Moiseenko F, Moiseyenko V: **Tumor acidity: From hallmark of cancer to target of treatment**. *Front Oncol* 2022, **12**:979154.
45. Jiang M, Wang Y, Zhao X, Yu J: **From metabolic byproduct to immune modulator: the role of lactate in tumor immune escape**. *Front Immunol* 2024, **15**:1492050.
46. Brown RB: **Cancer Cachexia and Dysregulated Phosphate Metabolism: Insights from Mutant p53 and Mutant Klotho Mouse Models**. *Metabolites* 2022, **12**(12).
47. Kelley RK, Joseph NM, Nimeiri HS, Hwang J, Kulik LM, Ngo Z, Behr SC, Onodera C, Zhang K, Bocobo AG *et al*: **Phase II Trial of the Combination of Temsirolimus and Sorafenib in Advanced Hepatocellular Carcinoma with Tumor Mutation Profiling**. *Liver Cancer* 2021, **10**(6):561-571.
48. Zavaglia C, Airoldi A, Mancuso A, Vangeli M, Vigano R, Cordone G, Gentiluomo M, Belli LS: **Adverse events affect sorafenib efficacy in patients with recurrent hepatocellular carcinoma after liver transplantation: experience at a single center and review of the literature**. *Eur J Gastroenterol Hepatol* 2013, **25**(2):180-186.
49. Yishake D, He TT, Liu ZY, Chen S, Luo Y, Liu XZ, Huang RZ, Lan QY, Fang AP, Zhu HL: **Dietary protein and prognosis of hepatocellular carcinoma: a prospective cohort study**. *Food Funct* 2021, **12**(22):11568-11576.
50. Nakashima J, Tachibana M, Ueno M, Miyajima A, Baba S, Murai M: **Association between tumor necrosis factor in serum and cachexia in patients with prostate cancer**. *Clin Cancer Res* 1998, **4**(7):1743-1748.
51. He Y, Ren T, Ji C, Zhao L, Wang X: **The baseline hemoglobin level is a positive biomarker for immunotherapy response and can improve the predictability of tumor mutation burden for immunotherapy response in cancer**. *Front Pharmacol* 2024, **15**:1456833.
52. Zhou J, Yang D: **Prognostic Significance of Hemoglobin, Albumin, Lymphocyte and Platelet (HALP) Score in Hepatocellular Carcinoma**. *J Hepatocell Carcinoma* 2023, **10**:821-831.

Figure Legends

Graphical Abstract. This figure illustrates the study design and key findings.



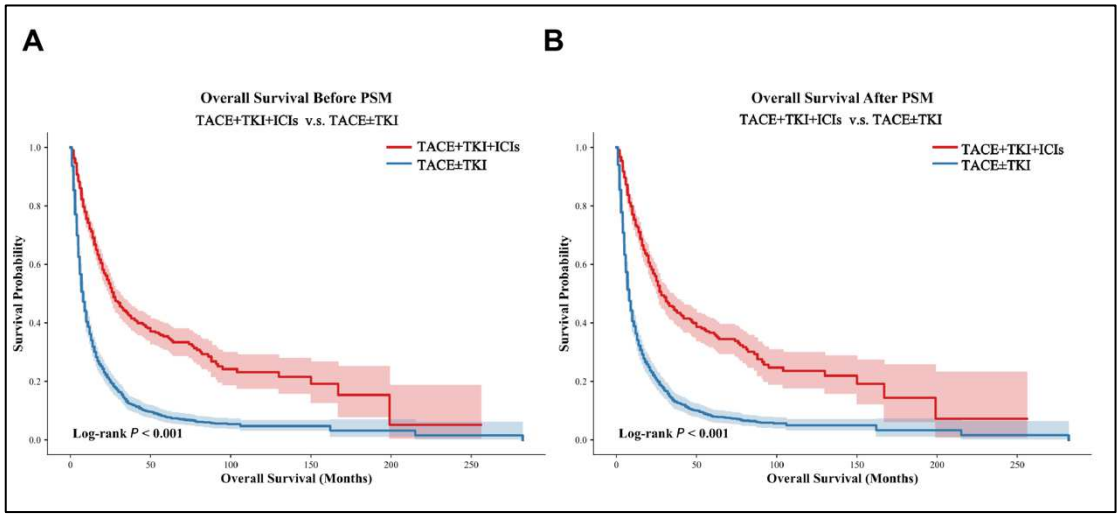


Figure 1. Overall survival of synchronous triple therapy versus pre-immunotherapy TACE before and after propensity score matching. (A) Kaplan-Meier curves comparing overall survival between patients receiving synchronous triple therapy (TACE plus TKIs and ICIs, n=1,001) and those in the pre-immunotherapy TACE group (n=791) before propensity score matching. The log-rank P value was less than 0.001. (B) Kaplan-Meier curves comparing overall survival between the two groups after 1:1 propensity score matching (n=716 per group). Patients receiving synchronous triple therapy demonstrated significantly superior overall survival compared with those in the pre-immunotherapy TACE group (median, 28.0 vs. 8.0 months; log-rank P < 0.001).

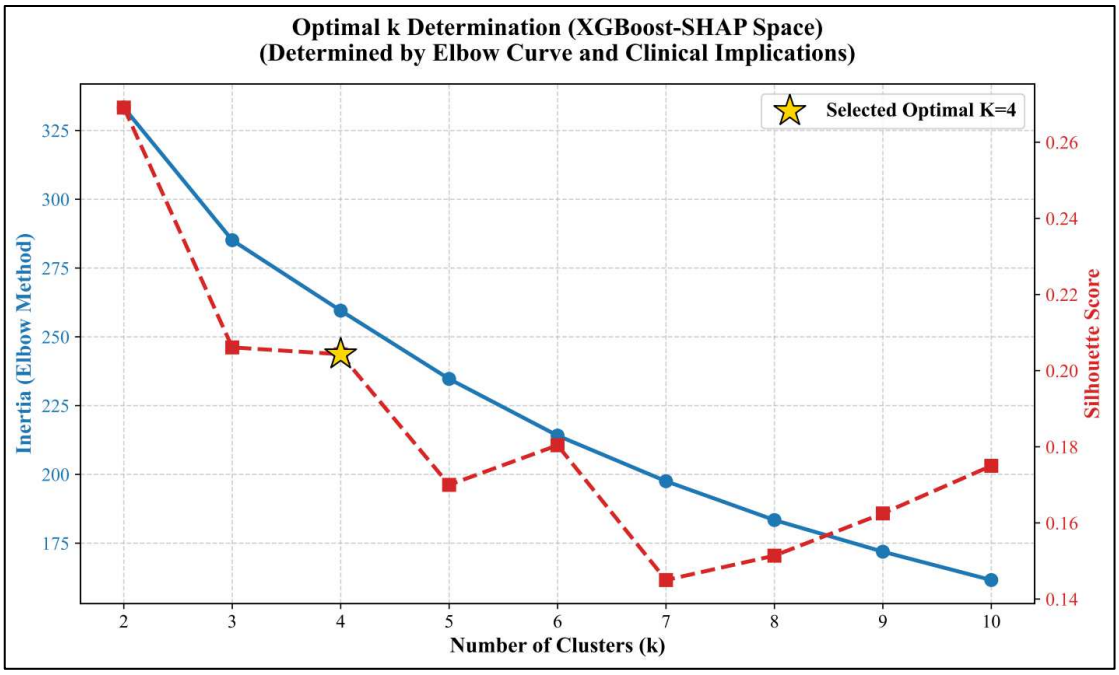


Figure 2. Optimal cluster number determination. Evaluation of inertia (elbow method) and Silhouette score across cluster numbers from 2 to 10. The inertia curve demonstrated a distinct elbow at K=4, and the Silhouette score confirmed optimal separation at this configuration. K=4 was selected as the optimal clustering configuration.

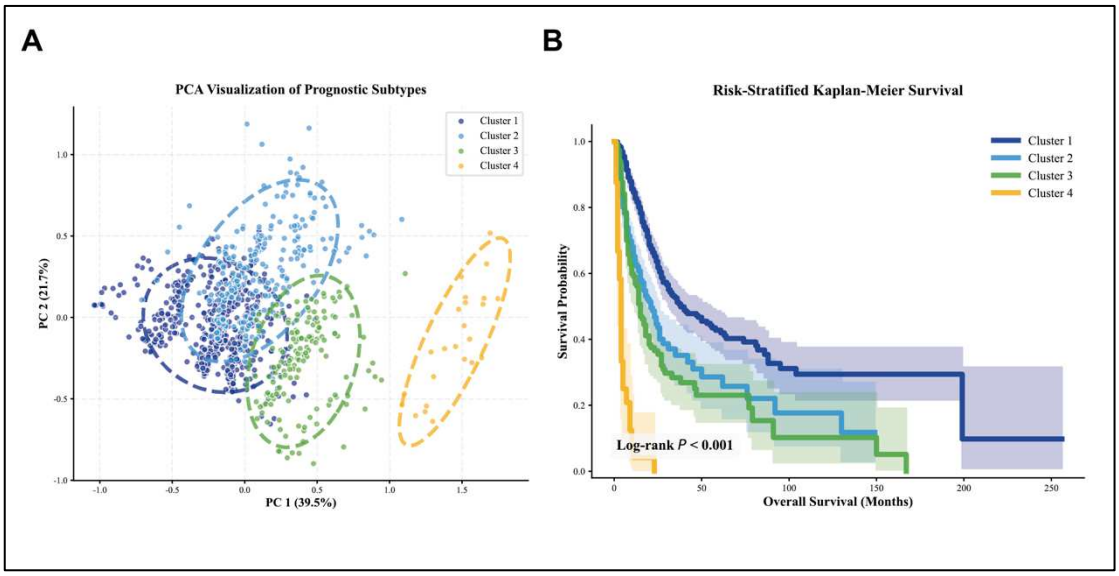


Figure 3. Subtype integrity validated by PCA and survival analysis. (A) Principal component analysis of the SHAP space demonstrating robust spatial segregation of the four clusters, with 95% confidence ellipses confirming structural integrity. (B) Kaplan-Meier survival curves of the four clusters identified by SHAP-driven K-means clustering, showing a stepwise survival gradient from the metabolically fit phenotype (Cluster 1) to the metabolically exhausted phenotype (Cluster 4). The log-rank P value was less than 0.001.

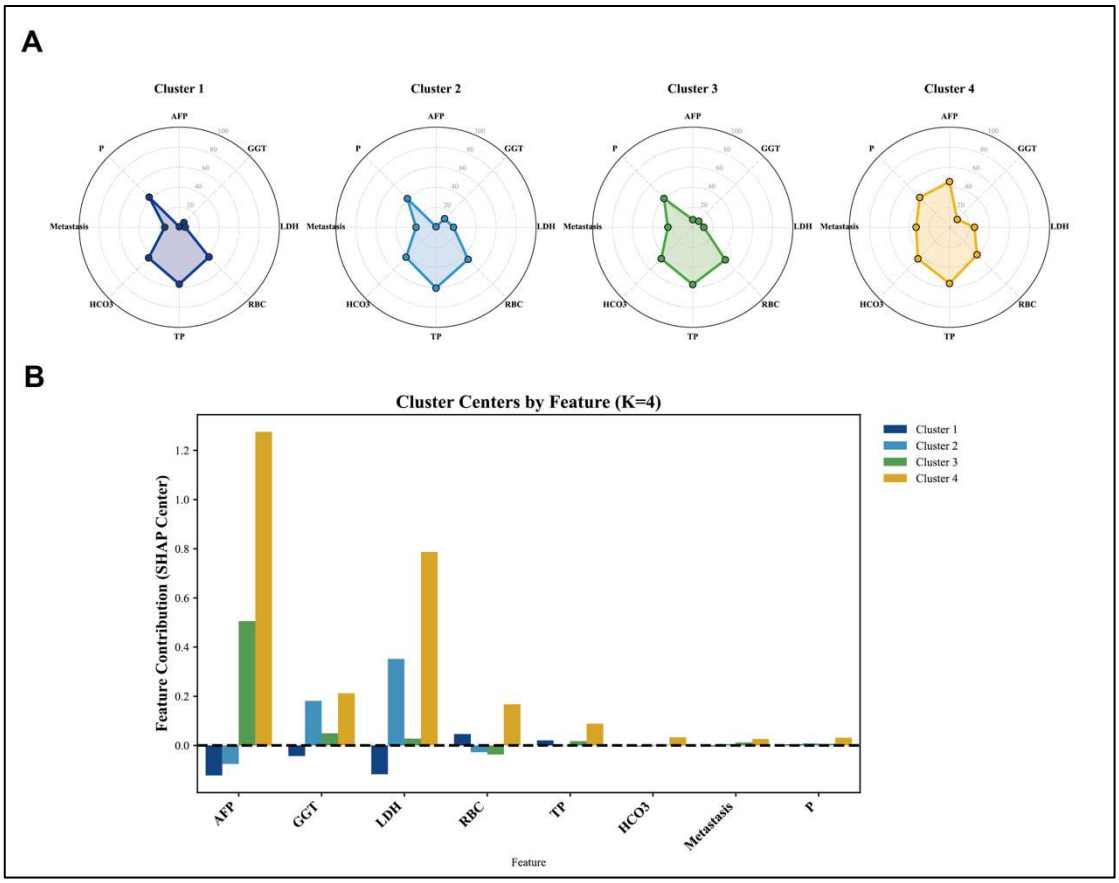


Figure 4. Phenotypic architecture of the four clusters. (A) Radar plots illustrating the standardized feature values across the eight core features for each cluster. (B) Cluster-specific SHAP signature centers showing the mean SHAP value for each feature across the four clusters. The metabolically fit phenotype (Cluster 1) demonstrated protective (negative) SHAP contributions across all features, while the metabolically exhausted phenotype (Cluster 4) demonstrated risk-increasing (positive) SHAP contributions for AFP, GGT, LDH, and metastasis.

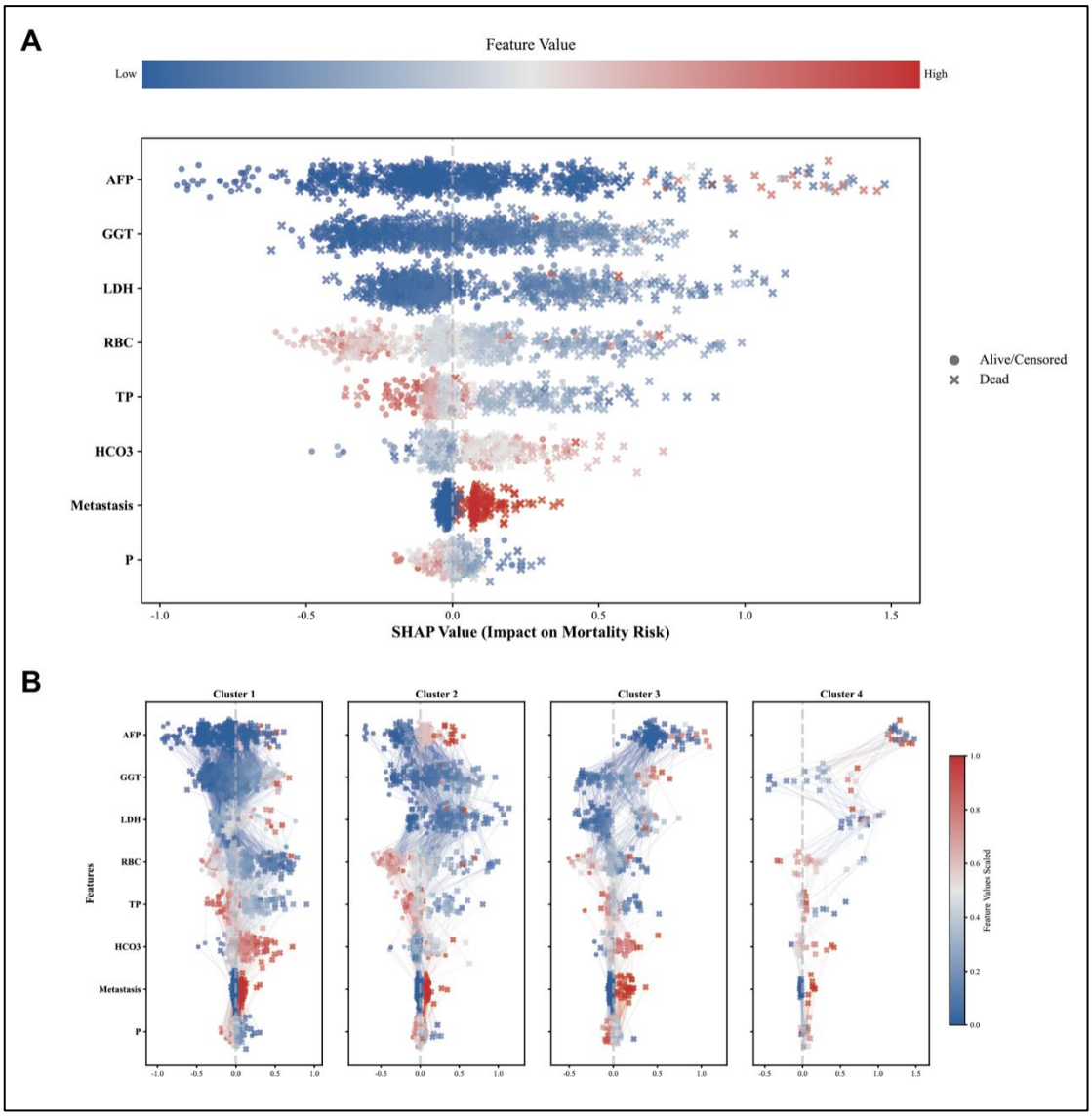


Figure 5. SHAP global and cluster-specific interpretability. (A) SHAP event stratification scatter plot showing feature contributions to mortality risk stratified by clinical endpoint (Alive/Censored vs. Dead). Deceased patients were concentrated in high-positive SHAP domains, driven by elevated AFP, GGT, and LDH and suppressed bicarbonate, total protein, phosphorus, and RBC. Red indicates high feature values; blue indicates low feature values. (B) SHAP cluster trajectory facets showing the distribution of scaled feature values across the four clusters. Each facet represents one cluster, with feature values scaled from 0 to 1. The orderly transition from protective feature profiles in Cluster 1 to risk-increasing profiles in Cluster 4 is clearly demonstrated.

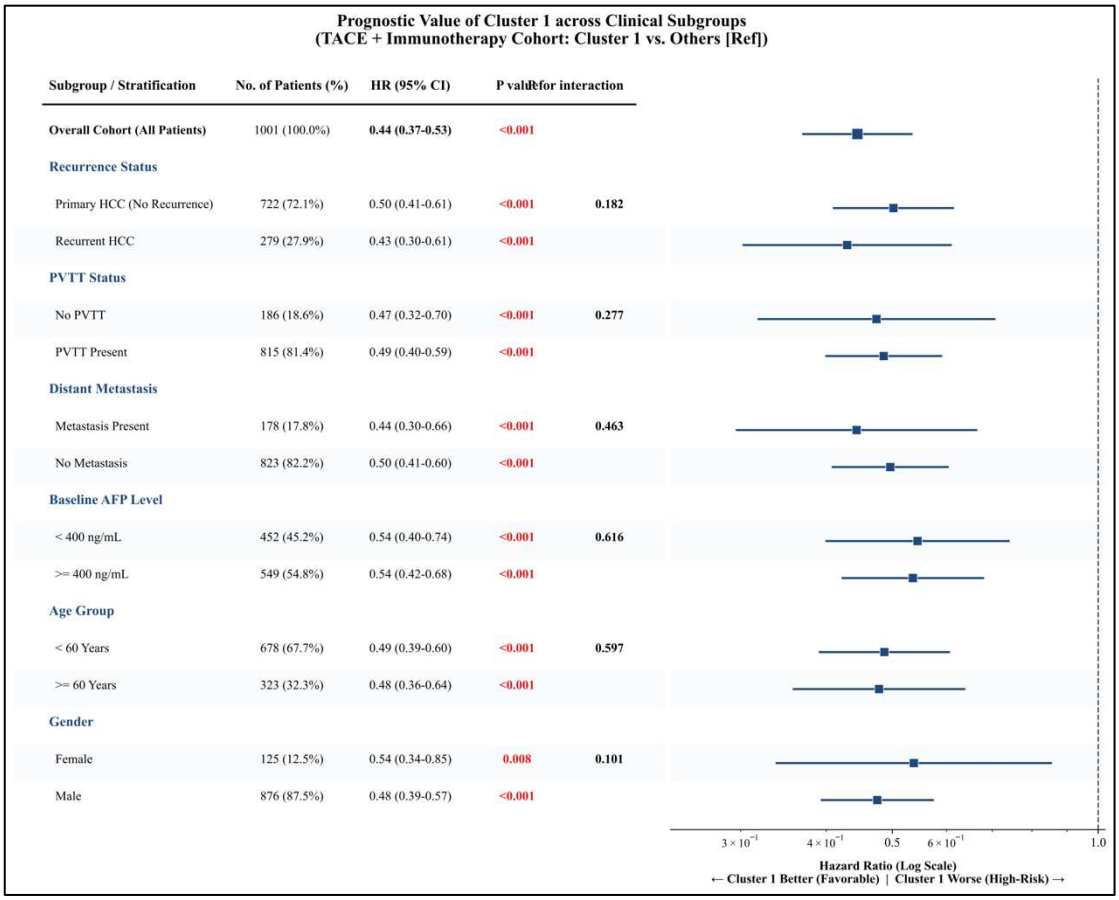


Figure 6. Subgroup validation of the metabolically fit phenotype (Cluster 1 vs. others). Forest plot showing the favorable prognosis associated with Cluster 1 across all clinical strata, with all P for interaction exceeding 0.05. HRs are shown on a logarithmic scale.

Supplementary Figure Legends

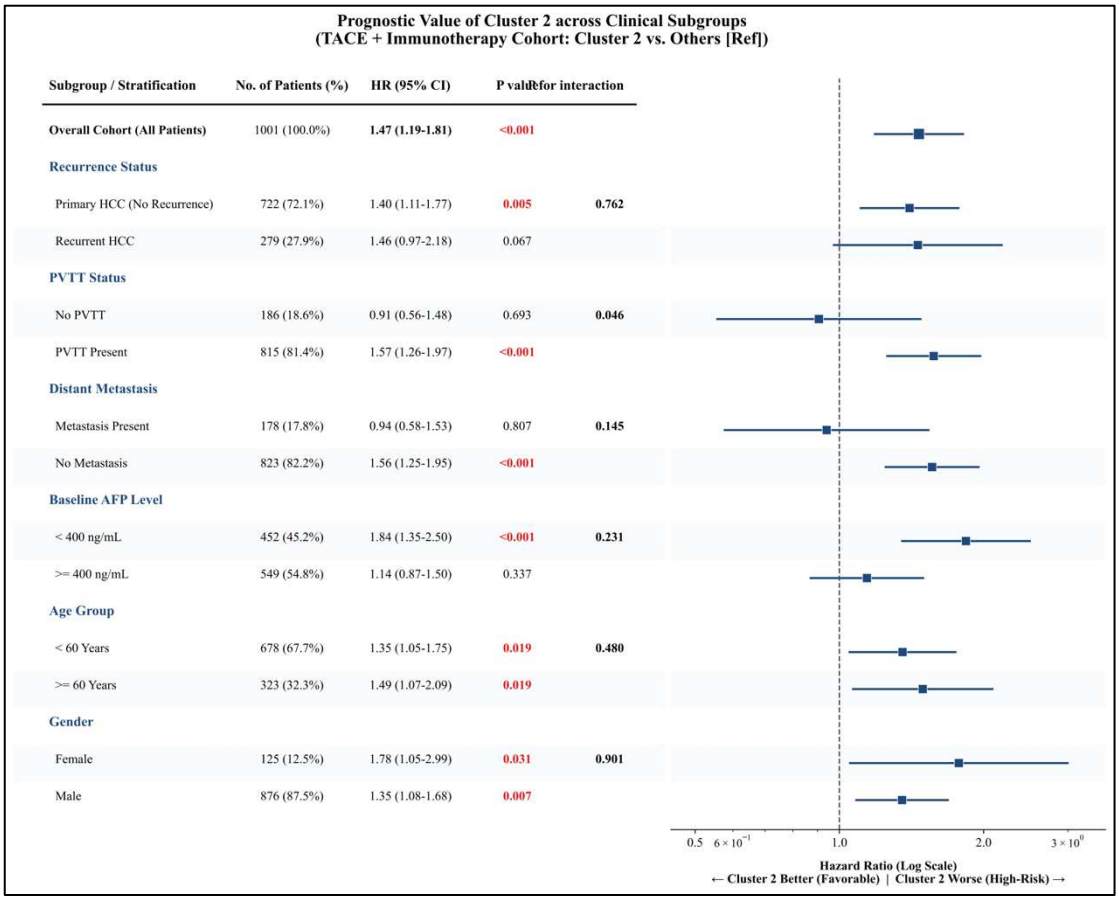


Figure S1. Subgroup validation of the metabolically fit phenotype (Cluster 2 vs. others). Forest plot showing the favorable prognosis associated with Cluster 2 across all clinical strata. HRs are shown on a logarithmic scale.

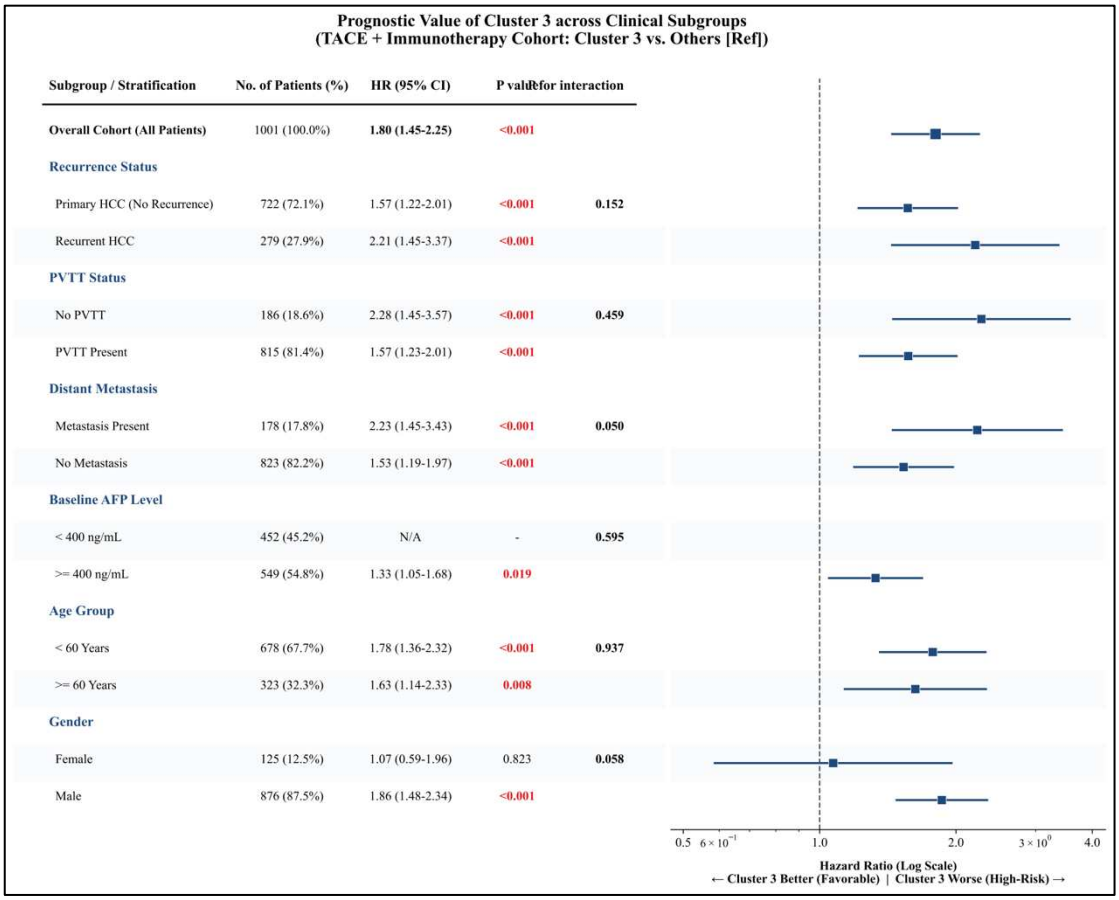


Figure S2. Subgroup validation of the metabolically fit phenotype (Cluster 3 vs. others). Forest plot showing the favorable prognosis associated with Cluster 3 across all clinical strata. HRs are shown on a logarithmic scale.

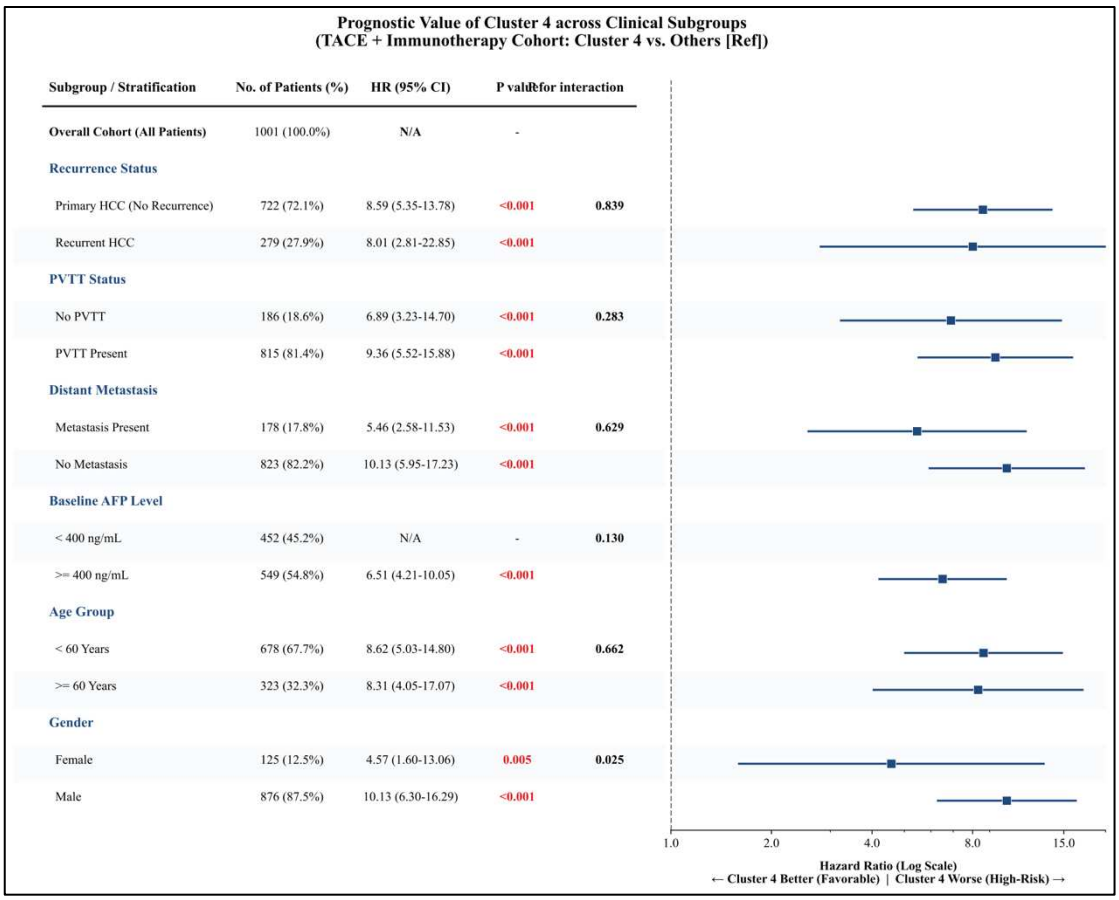


Figure S3. Subgroup validation of the metabolically fit phenotype (Cluster 4 vs. others). Forest plot showing the favorable prognosis associated with Cluster 3 across all clinical strata. HRs are shown on a logarithmic scale.

Tables

Table 1. Univariate and multivariate Cox proportional hazards analysis.

Characteristics	*Univariate HR (95% CI)*	*Univariate P-value*	*Multivariate HR (95% CI)*	*Multivariate P-value*
AFP	**1.219 (1.147-1.295)**	**<0.001**	**1.178 (1.097-1.266)**	**<0.001**
TP	**0.886 (0.807-0.972)**	**0.011**	**0.846 (0.760-0.940)**	**0.002**
GGT	**1.208 (1.133-1.288)**	**<0.001**	**1.130 (1.026-1.245)**	**0.013**
LDH	**1.189 (1.114-1.269)**	**<0.001**	**1.140 (1.024-1.271)**	**0.017**
P	**0.903 (0.823-0.990)**	**0.030**	**0.882 (0.794-0.980)**	**0.019**
Metastasis				
No	Reference	-	Reference	-
Yes	**1.458 (1.160-1.831)**	**0.001**	**1.329 (1.035-1.705)**	**0.026**
HCO3	**1.153 (1.047-1.269)**	**0.004**	**1.170 (1.012-1.353)**	**0.034**
RBC	**0.831 (0.753-0.917)**	**<0.001**	**0.874 (0.765-0.999)**	**0.048**
Cl	0.666 (0.608-0.731)	<0.001	0.842 (0.698-1.017)	0.075
Anion_Gap	1.210 (1.110-1.320)	<0.001	1.141 (0.977-1.334)	0.095
K	1.115 (1.018-1.222)	0.019	1.087 (0.978-1.207)	0.123
TBIL	1.178 (1.106-1.254)	<0.001	1.085 (0.976-1.207)	0.129
CHE	0.699 (0.632-0.773)	<0.001	0.894 (0.773-1.034)	0.131
NLR	1.083 (1.011-1.161)	0.024	0.927 (0.832-1.034)	0.174
AST	1.252 (1.169-1.341)	<0.001	1.076 (0.966-1.197)	0.182
ADA	1.183 (1.096-1.278)	<0.001	1.067 (0.956-1.191)	0.245
ALB	0.754 (0.689-0.825)	<0.001	0.932 (0.810-1.071)	0.322
PCT	1.114 (1.013-1.225)	0.025	1.054 (0.941-1.180)	0.367
GLDH	1.081 (1.008-1.159)	0.030	0.948 (0.842-1.066)	0.373
EOS#	0.896 (0.806-0.996)	0.042	0.923 (0.772-1.103)	0.378
PA	0.707 (0.642-0.778)	<0.001	0.935 (0.787-1.112)	0.447
BUN	0.864 (0.778-0.960)	0.006	0.961 (0.850-1.086)	0.522
LAP	1.151 (1.089-1.217)	<0.001	1.026 (0.941-1.119)	0.562
HGB	0.858 (0.784-0.940)	0.001	0.945 (0.777-1.150)	0.573
Na	0.835 (0.759-0.919)	<0.001	1.038 (0.885-1.219)	0.645
INR	1.120 (1.021-1.230)	0.016	0.970 (0.844-1.114)	0.665
MONO	1.148 (1.047-1.259)	0.003	1.021 (0.914-1.141)	0.709
Cr	0.867 (0.772-0.972)	0.015	1.022 (0.907-1.151)	0.720
ALP	1.065 (1.014-1.119)	0.011	0.986 (0.892-1.090)	0.787
HCT	0.849 (0.773-0.933)	<0.001	1.023 (0.832-1.259)	0.827
MAO	1.128 (1.033-1.231)	0.007	1.011 (0.892-1.147)	0.864
RBP	0.760 (0.687-0.839)	<0.001	1.013 (0.862-1.191)	0.873

TBA	1.091 (1.010-1.179)	0.028	0.995 (0.896-1.105)	0.923
PT	1.127 (1.025-1.239)	0.014	0.996 (0.877-1.131)	0.954
MCH	1.088 (0.989-1.196)	0.083	-	-
APTT	0.922 (0.834-1.019)	0.110	-	-
MPV	1.074 (0.984-1.173)	0.112	-	-
Mg	1.071 (0.984-1.165)	0.113	-	-
PLT	1.079 (0.981-1.188)	0.118	-	-
P-LCR	1.065 (0.976-1.162)	0.159	-	-
MCV	1.069 (0.973-1.174)	0.166	-	-
TRF	0.938 (0.855-1.030)	0.180	-	-
MCHC	1.059 (0.964-1.164)	0.233	-	-
FER	1.049 (0.964-1.141)	0.265	-	-
UA	0.952 (0.865-1.047)	0.312	-	-
LPS	1.048 (0.956-1.150)	0.318	-	-
BASO	1.043 (0.960-1.134)	0.321	-	-
CysC	1.040 (0.954-1.135)	0.374	-	-
ALT	1.034 (0.954-1.120)	0.413	-	-
TT	1.036 (0.942-1.139)	0.468	-	-
Ca	1.023 (0.930-1.126)	0.635	-	-
FIB	1.020 (0.933-1.114)	0.667	-	-
PDW	1.013 (0.929-1.105)	0.773	-	-
Age	0.868 (0.786-0.959)	0.006	0.904 (0.811-1.008)	0.071
Gender				
Female	Reference	-	-	-
Male	0.876 (0.676-1.135)	0.316	-	-
PVTT				
No	Reference	-	-	-
Yes	0.855 (0.681-1.073)	0.176	-	-
Recurrence				
No	Reference	-	Reference	-
Yes	0.767 (0.621-0.947)	0.014	0.891 (0.710-1.118)	0.317

AFP: Alpha-Fetoprotein; TP: Total Protein; GGT: Gamma-Glutamyl Transferase; LDH: Lactate Dehydrogenase; P: Phosphorus; HCO3: Bicarbonate; RBC: Red Blood Cell Count; Cl: Chloride; Anion_Gap: Anion Gap; K: Potassium; TBIL: Total Bilirubin; CHE: Cholinesterase; NLR: Neutrophil-to-Lymphocyte Ratio; AST: Aspartate Aminotransferase; ADA: Adenosine Deaminase; ALB: Albumin; PCT: Procalcitonin; GLDH: Glutamate Dehydrogenase; EOS: Eosinophil Count; PA: Prealbumin; BUN: Blood Urea Nitrogen; LAP: Leucine Aminopeptidase; HGB: Hemoglobin; Na: Sodium; INR: International Normalized Ratio; MONO: Monocyte Count; Cr: Creatinine; ALP: Alkaline Phosphatase; HCT: Hematocrit; MAO: Monoamine Oxidase; RBP: Retinol-Binding Protein; TBA: Total Bile Acid; PT: Prothrombin Time; MCH: Mean Corpuscular Hemoglobin; APTT: Activated Partial Thromboplastin Time; MPV: Mean Platelet Volume; Mg: Magnesium; PLT: Platelet Count; P-LCR: Platelet-Large Cell Ratio;

MCV: Mean Corpuscular Volume; TRF: Transferrin; MCHC: Mean Corpuscular Hemoglobin Concentration; FER: Ferritin; UA: Uric Acid; LPS: Lipase; BASO: Basophil Count; CysC: Cystatin C; ALT: Alanine Aminotransferase; TT: Thrombin Time; Ca: Calcium; FIB: Fibrinogen; PDW: Platelet Distribution Width; WBC: White Blood Cell Count; LYM: Lymphocyte Count; NEU: Neutrophil Count; AST_ALT_Ratio: AST to ALT Ratio; A_G_Ratio: Albumin to Globulin Ratio; DBIL: Direct Bilirubin; IBIL: Indirect Bilirubin; GLB: Globulin; Gender: Sex; Metastasis: Distant Metastasis; PVTT: Portal Vein Tumor Thrombus; CI: Confidence Interval; HR: Hazard Ratio.

Table 2. Comprehensive survival summary of the four clusters.

Cohort	*Subgroup*	*N*	*Events*	*Median OS, Months (95% CI)*	*1-Year OS Rate (95% CI)*	*3-Year OS Rate (95% CI)*	*5-Year OS Rate (95% CI)*	*Log-rank P*
Triple therapy (TACE+TKIs +ICIs）	Cluster 1	586	231	38.0 (31.0-55.0)	82.7% (79.2-85.6%)	51.2% (45.8-56.3%)	42.7% (36.8-48.6%)	< 0.001
	Cluster 2	246	115	21.0 (16.0-26.0)	62.7% (55.6-69.0%)	35.1% (26.2-44.2%)	28.6% (19.1-38.8%)	
	Cluster 3	145	101	15.0 (12.0-18.0)	56.9% (48.3-64.6%)	28.4% (20.3-37.0%)	23.1% (14.9-32.2%)	
	Cluster 4	24	24	4.0 (2.0-5.0)	4.2% (0.3-17.6%)	N/A	N/A	

Supplementary Tables

Table S1. Baseline characteristics before and after propensity score matching.

Characteristics	Before PSM			After PSM		
	Synchronous TACE+TKI+ICI (N=1001)	***TACE±TKI (N=791)***	***P-value***	***Synchronous TACE+TKI+ICI (N=716)***	***TACE±TKI (N=716)***	***P-value***
Age (Mean ± SD)	52.85 ± 11.10	51.40 ± 11.10	0.007	52.92 ± 11.13	51.42 ± 10.97	0.012
Gender, n (%)			0.632			0.619
Female	125 (12.5%)	92 (11.6%)		86 (12.0%)	79 (11.0%)	
Male	876 (87.5%)	699 (88.4%)		630 (88.0%)	637 (89.0%)	
PVTT, n (%)			0.343			0.199
No	186 (18.6%)	162 (20.5%)		108 (15.1%)	127 (17.7%)	
Yes	815 (81.4%)	629 (79.5%)		608 (84.9%)	589 (82.3%)	
Metastasis, n (%)			0.001			0.034
No	823 (82.2%)	601 (76.0%)		611 (85.3%)	580 (81.0%)	
Yes	178 (17.8%)	190 (24.0%)		105 (14.7%)	136 (19.0%)	
Recurrence, n (%)			<0.001			0.061
No	722 (72.1%)	745 (94.2%)		650 (90.8%)	670 (93.6%)	
Yes	279 (27.9%)	46 (5.8%)		66 (9.2%)	46 (6.4%)	
ADA (Mean ± SD)	25.85 ± 11.03	24.89 ± 10.96	0.066	25.68 ± 10.34	24.92 ± 11.04	0.180

AFP (Mean ± SD)	3653.51 ± 16535.29	815.13 ± 825.77	<0.001	1211.09 ± 6321.68	814.90 ± 819.73	0.097
ALB (Mean ± SD)	34.99 ± 4.95	34.96 ± 4.70	0.923	35.00 ± 4.98	34.93 ± 4.65	0.795
ALP (Mean ± SD)	172.06 ± 158.97	155.24 ± 116.95	0.010	174.13 ± 178.25	153.58 ± 118.22	0.010
ALT (Mean ± SD)	48.86 ± 46.74	55.69 ± 60.56	0.009	49.95 ± 46.61	55.82 ± 60.89	0.041
APTT (Mean ± SD)	34.89 ± 6.90	30.88 ± 5.99	<0.001	34.47 ± 6.94	30.77 ± 6.08	<0.001
AST (Mean ± SD)	89.20 ± 84.49	89.92 ± 91.67	0.865	88.74 ± 83.50	88.72 ± 88.78	0.995
AST_ALT_Ratio (Mean ± SD)	2.17 ± 1.78	2.16 ± 7.21	0.990	2.08 ± 1.65	2.17 ± 7.56	0.762
A_G_Ratio (Mean ± SD)	1.12 ± 0.42	1.11 ± 0.28	0.483	1.13 ± 0.45	1.11 ± 0.28	0.237
Anion_Gap (Mean ± SD)	11.05 ± 2.85	12.53 ± 2.78	<0.001	11.17 ± 2.85	12.46 ± 2.67	<0.001
BASO# (Mean ± SD)	0.036 ± 0.024	0.039 ± 0.067	0.132	0.036 ± 0.026	0.036 ± 0.024	0.859
BUN (Mean ± SD)	4.69 ± 1.86	4.81 ± 1.85	0.158	4.75 ± 1.97	4.78 ± 1.77	0.772
CHE (Mean ± SD)	5427.77 ± 2227.33	5305.13 ± 2058.87	0.227	5447.92 ± 2276.91	5295.13 ± 2064.70	0.184
Ca (Mean ± SD)	2.21 ± 0.14	2.32 ± 0.21	<0.001	2.21 ± 0.15	2.32 ± 0.20	<0.001
Cl (Mean ± SD)	102.92 ± 3.71	101.42 ± 3.45	<0.001	102.80 ± 3.67	101.52 ± 3.42	<0.001
Cr (Mean ± SD)	72.72 ± 22.90	74.62 ± 25.38	0.100	73.98 ± 24.96	73.94 ± 22.06	0.972
CysC (Mean ± SD)	1.03 ± 0.27	1.03 ± 0.29	0.929	1.03 ± 0.27	1.03 ± 0.27	0.624
DBIL (Mean ± SD)	8.99 ± 8.79	9.99 ± 18.15	0.156	9.31 ± 9.70	9.45 ± 8.88	0.781
EOS (Mean ± SD)	0.254 ± 0.323	0.301 ± 0.528	0.027	0.261 ± 0.331	0.295 ± 0.518	0.136
FER (Mean ± SD)	609.50 ± 511.45	420.50 ± 284.79	<0.001	594.09 ± 495.27	419.45 ± 288.61	<0.001
FIB (Mean ± SD)	3.68 ± 1.29	3.51 ± 1.37	0.009	3.68 ± 1.34	3.43 ± 1.33	<0.001
GGT (Mean ± SD)	183.35 ± 170.42	199.10 ± 168.83	0.051	180.48 ± 158.52	197.18 ± 169.70	0.055

GLB (Mean ± SD)	33.27 ± 7.10	32.93 ± 6.13	0.277	32.97 ± 6.93	32.96 ± 6.24	0.964
GLDH (Mean ± SD)	26.75 ± 62.83	25.51 ± 57.50	0.665	26.73 ± 68.66	25.04 ± 56.42	0.609
HCO3 (Mean ± SD)	24.95 ± 2.50	25.87 ± 2.48	<0.001	24.95 ± 2.45	25.91 ± 2.43	<0.001
HCT (Mean ± SD)	39.05 ± 6.54	39.77 ± 6.70	0.024	39.24 ± 6.43	39.57 ± 6.62	0.336
HGB (Mean ± SD)	127.25 ± 22.60	129.24 ± 22.87	0.066	127.91 ± 22.50	128.68 ± 22.71	0.521
IBIL (Mean ± SD)	10.77 ± 5.44	11.26 ± 6.37	0.087	11.00 ± 5.79	11.17 ± 5.94	0.598
INR (Mean ± SD)	1.07 ± 0.13	1.10 ± 0.14	<0.001	1.07 ± 0.13	1.09 ± 0.14	0.005
K (Mean ± SD)	3.96 ± 0.45	4.20 ± 0.49	<0.001	3.96 ± 0.46	4.20 ± 0.50	<0.001
LAP (Mean ± SD)	59.54 ± 37.49	57.16 ± 30.35	0.138	58.94 ± 33.49	57.00 ± 30.97	0.254
LDH (Mean ± SD)	288.39 ± 196.56	328.96 ± 307.35	0.001	281.10 ± 184.53	325.27 ± 312.67	0.001
LPS (Mean ± SD)	50.27 ± 35.88	43.68 ± 41.72	<0.001	50.15 ± 34.06	43.77 ± 40.61	0.001
MAO (Mean ± SD)	6.28 ± 3.54	5.65 ± 2.86	<0.001	6.11 ± 3.30	5.50 ± 2.70	<0.001
MCH (Mean ± SD)	28.95 ± 4.99	28.99 ± 3.75	0.832	28.92 ± 3.93	29.07 ± 3.74	0.468
MCHC (Mean ± SD)	325.90 ± 31.82	324.43 ± 10.71	0.172	325.30 ± 11.20	324.54 ± 10.65	0.187
MCV (Mean ± SD)	88.63 ± 10.65	89.23 ± 10.15	0.225	88.74 ± 10.64	89.44 ± 10.13	0.206
MONO (Mean ± SD)	0.509 ± 0.219	0.570 ± 0.274	<0.001	0.511 ± 0.230	0.562 ± 0.271	<0.001
MPV (Mean ± SD)	9.37 ± 1.05	9.56 ± 1.06	<0.001	9.39 ± 1.07	9.57 ± 1.07	0.002
Mg (Mean ± SD)	0.837 ± 0.113	0.886 ± 0.150	<0.001	0.845 ± 0.114	0.883 ± 0.150	<0.001
Na (Mean ± SD)	138.89 ± 2.88	139.82 ± 3.21	<0.001	138.90 ± 2.90	139.88 ± 3.14	<0.001
P (Mean ± SD)	1.05 ± 0.18	1.02 ± 0.19	<0.001	1.05 ± 0.18	1.01 ± 0.18	0.001
P-LCR (Mean ± SD)	23.05 ± 7.28	23.86 ± 7.52	0.021	23.16 ± 7.44	23.94 ± 7.54	0.048
PA (Mean ± SD)	147.20 ± 55.54	132.69 ± 54.44	<0.001	148.08 ± 54.57	132.15 ± 53.81	<0.001
PCT (Mean ± SD)	0.182 ± 0.090	0.205 ± 0.094	<0.001	0.182 ± 0.092	0.198 ± 0.082	<0.001
PDW (Mean ± SD)	15.92 ± 0.47	15.89 ± 0.41	0.086	15.92 ± 0.49	15.89 ± 0.41	0.250

PLT (Mean ± SD)	198.58 ± 106.21	218.95 ± 106.39	<0.001	199.17 ± 110.20	210.67 ± 95.51	0.035
PT (Mean ± SD)	12.64 ± 1.93	13.16 ± 1.66	<0.001	12.71 ± 1.98	13.07 ± 1.62	<0.001
RBC (Mean ± SD)	4.45 ± 0.83	4.51 ± 0.87	0.203	4.47 ± 0.82	4.47 ± 0.85	0.983
RBP (Mean ± SD)	23.09 ± 11.22	30.56 ± 13.74	<0.001	23.30 ± 11.13	30.38 ± 13.47	<0.001
TBA (Mean ± SD)	21.90 ± 27.53	21.70 ± 31.39	0.891	22.39 ± 29.10	21.80 ± 31.17	0.709
TBIL (Mean ± SD)	19.76 ± 12.90	21.25 ± 22.55	0.099	20.31 ± 14.03	20.61 ± 13.52	0.680
TP (Mean ± SD)	68.26 ± 6.92	67.90 ± 6.63	0.259	67.97 ± 6.94	67.89 ± 6.66	0.820
TRF (Mean ± SD)	2.03 ± 0.46	2.19 ± 0.59	<0.001	2.04 ± 0.47	2.20 ± 0.59	<0.001
TT (Mean ± SD)	18.32 ± 1.80	18.00 ± 5.30	0.103	18.40 ± 1.73	18.04 ± 5.53	0.097
UA (Mean ± SD)	323.82 ± 99.04	323.87 ± 101.49	0.992	324.83 ± 100.93	323.17 ± 97.69	0.752
NLR (Mean ± SD)	3.52 ± 3.33	3.58 ± 2.78	0.652	3.44 ± 3.10	3.47 ± 2.55	0.843

Table S2. Survival outcomes before and after propensity score matching.

Cohort	*Subgroup*	*N*	*Events*	*Median OS, Months (95% CI)*	*1-Year OS Rate (95% CI)*	*2-Year OS Rate (95% CI)*	*3-Year OS Rate (95% CI)*	*5-Year OS Rate (95% CI)*	*Log-rank P*
Before PSM	Synchronous TACE+TKI+ICI	1001	471	27.0 (24.0-31.0)	72.2% (69.1-75.0%)	53.5% (49.8-57.0%)	42.7% (38.7-46.7%)	35.4% (31.0-39.8%)	< 0.001
	Pre-immunotherapy TACE	791	752	8.0 (7.0-9.0)	36.2% (32.8-39.5%)	20.6% (17.9-23.5%)	12.5% (10.3-14.9%)	7.7% (6.0-9.7%)	
After PSM	Synchronous TACE+TKI+ICI	716	349	28.0 (26.0-35.0)	73.3% (69.8-76.5%)	56.0% (51.8-60.0%)	44.5% (39.9-48.9%)	36.7% (31.7-41.6%)	< 0.001
	Pre-immunotherapy TACE	716	679	8.0 (7.0-9.0)	36.3% (32.8-39.8%)	21.2% (18.3-24.3%)	13.1% (10.8-15.7%)	8.0% (6.1-10.1%)	

Table S3. Subgroup analysis for the metabolically fit phenotype (Cluster 1 vs. others).

Variable	*Strata*	*No. of Patients (%)*	*HR (95% CI)*	*P value*	*P for interaction*
Overall Cohort	All Patients	1001 (100.0%)	0.44 (0.37-0.53)	<0.001	-
Recurrence Status		-	-	-	-
	Primary HCC (No Recurrence)	722 (72.1%)	0.50 (0.41-0.61)	<0.001	0.182
	Recurrent HCC	279 (27.9%)	0.43 (0.30-0.61)	<0.001	-
PVTT Status		-	-	-	-
	No PVTT	186 (18.6%)	0.47 (0.32-0.70)	<0.001	0.277
	PVTT Present	815 (81.4%)	0.49 (0.40-0.59)	<0.001	-
Distant Metastasis		-	-	-	-
	Metastasis Present	178 (17.8%)	0.44 (0.30-0.66)	<0.001	0.463
	No Metastasis	823 (82.2%)	0.50 (0.41-0.60)	<0.001	-
Baseline AFP Level		-	-	-	-
	< 400 ng/mL	452 (45.2%)	0.54 (0.40-0.74)	<0.001	0.616
	>= 400 ng/mL	549 (54.8%)	0.54 (0.42-0.68)	<0.001	-
Age Group		-	-	-	-
	< 60 Years	678 (67.7%)	0.49 (0.39-0.60)	<0.001	0.597
	>= 60 Years	323 (32.3%)	0.48 (0.36-0.64)	<0.001	-
Gender		-	-	-	-
	Female	125 (12.5%)	0.54 (0.34-0.85)	0.008	0.101
	Male	876 (87.5%)	0.48 (0.39-0.57)	<0.001	-

Table S4. Subgroup analysis for the metabolically compensated phenotype (Cluster 2 vs. others).

Variable	*Strata*	*No. of Patients (%)*	*HR (95% CI)*	*P value*	*P for interaction*
Overall Cohort	All Patients	1001 (100.0%)	1.47 (1.19-1.81)	<0.001	-
Recurrence Status		-	-	-	-
	Primary HCC (No Recurrence)	722 (72.1%)	1.40 (1.11-1.77)	0.005	0.762
	Recurrent HCC	279 (27.9%)	1.46 (0.97-2.18)	0.067	-
PVTT Status		-	-	-	-
	No PVTT	186 (18.6%)	0.91 (0.56-1.48)	0.693	0.046
	PVTT Present	815 (81.4%)	1.57 (1.26-1.97)	<0.001	-
Distant Metastasis		-	-	-	-
	Metastasis Present	178 (17.8%)	0.94 (0.58-1.53)	0.807	0.145
	No Metastasis	823 (82.2%)	1.56 (1.25-1.95)	<0.001	-
Baseline AFP Level		-	-	-	-
	< 400 ng/mL	452 (45.2%)	1.84 (1.35-2.50)	<0.001	0.231
	>= 400 ng/mL	549 (54.8%)	1.14 (0.87-1.50)	0.337	-
Age Group		-	-	-	-
	< 60 Years	678 (67.7%)	1.35 (1.05-1.75)	0.019	0.480
	>= 60 Years	323 (32.3%)	1.49 (1.07-2.09)	0.019	-
Gender		-	-	-	-
	Female	125 (12.5%)	1.78 (1.05-2.99)	0.031	0.901
	Male	876 (87.5%)	1.35 (1.08-1.68)	0.007	-

Table S5. Subgroup analysis for the tumor-metabolism dominant phenotype (Cluster 3 vs. others).

Variable	*Strata*	*No. of Patients (%)*	*HR (95% CI)*	*P value*	*P for interaction*
Overall Cohort	All Patients	1001 (100.0%)	1.80 (1.45-2.25)	<0.001	-
Recurrence Status		-	-	-	-
	Primary HCC (No Recurrence)	722 (72.1%)	1.57 (1.22-2.01)	<0.001	0.152
	Recurrent HCC	279 (27.9%)	2.21 (1.45-3.37)	<0.001	-
PVTT Status		-	-	-	-
	No PVTT	186 (18.6%)	2.28 (1.45-3.57)	<0.001	0.459
	PVTT Present	815 (81.4%)	1.57 (1.23-2.01)	<0.001	-
Distant Metastasis		-	-	-	-
	Metastasis Present	178 (17.8%)	2.23 (1.45-3.43)	<0.001	0.050
	No Metastasis	823 (82.2%)	1.53 (1.19-1.97)	<0.001	-
Baseline AFP Level		-	-	-	-
	< 400 ng/mL	452 (45.2%)	-	-	0.595
	>= 400 ng/mL	549 (54.8%)	1.33 (1.05-1.68)	0.019	-
Age Group		-	-	-	-
	< 60 Years	678 (67.7%)	1.78 (1.36-2.32)	<0.001	0.937
	>= 60 Years	323 (32.3%)	1.63 (1.14-2.33)	0.008	-
Gender		-	-	-	-
	Female	125 (12.5%)	1.07 (0.59-1.96)	0.823	0.058
	Male	876 (87.5%)	1.86 (1.48-2.34)	<0.001	-

Table S6. Subgroup analysis for the metabolically exhausted phenotype (Cluster 4 vs. others).

Variable	*Strata*	*No. of Patients (%)*	*HR (95% CI)*	*P value*	*P for interaction*
Overall Cohort	All Patients	1001 (100.0%)	-	-	-
Recurrence Status		-	-	-	-
	Primary HCC (No Recurrence)	722 (72.1%)	8.59 (5.35-13.78)	<0.001	0.839
	Recurrent HCC	279 (27.9%)	8.01 (2.81-22.85)	<0.001	-
PVTT Status		-	-	-	-
	No PVTT	186 (18.6%)	6.89 (3.23-14.70)	<0.001	0.283
	PVTT Present	815 (81.4%)	9.36 (5.52-15.88)	<0.001	-
Distant Metastasis		-	-	-	-
	Metastasis Present	178 (17.8%)	5.46 (2.58-11.53)	<0.001	0.629
	No Metastasis	823 (82.2%)	10.13 (5.95-17.23)	<0.001	-
Baseline AFP Level		-	-	-	-
	< 400 ng/mL	452 (45.2%)	-	-	0.130
	>= 400 ng/mL	549 (54.8%)	6.51 (4.21-10.05)	<0.001	-
Age Group		-	-	-	-
	< 60 Years	678 (67.7%)	8.62 (5.03-14.80)	<0.001	0.662
	>= 60 Years	323 (32.3%)	8.31 (4.05-17.07)	<0.001	-
Gender		-	-	-	-
	Female	125 (12.5%)	4.57 (1.60-13.06)	0.005	0.025
	Male	876 (87.5%)	10.13 (6.30-16.29)	<0.001	-